Quantitative profiling and mechanisms exploration of Epimedium total flavonoid capsules in neuroinflammation: An integrated study of pharmacokinetics, network pharmacology, and molecular pathways

Xiaochun Zeng [a,1], Junran Shao [a,1], Dabo Pan [d], Siying Zeng [a], Zhenzhong Wang [b,c], Xinsheng Yao [a], Haibo Li [b,c,*], Wei Xiao [b,c,*], Yang Yu [a,**]

[a] State Key Laboratory of Bioactive Molecules and Druggability Assessment, Guangdong Province Key Laboratory of Pharmacodynamic Constituents of TCM and New Drugs Research, International Cooperative Laboratory of Traditional Chinese Medicine Modernization and Innovative Drug Development of Ministry of Education (MOE) of China, Institute of Traditional Chinese Medicine & Natural Products, College of Pharmacy, Jinan University, Guangzhou 510632, China
[b] State Key Laboratory on Technologies for Chinese Medicine Pharmaceutical Process Control and Intelligent Manufacture, Jiangsu Kanion Pharmaceutical Co. Ltd., Jiangsu, Lianyungang, 222001, China
[c] School of Pharmacy, Nanjing University of Chinese Medicine, Nanjing 210023, China
[d] Department of Medical Technology, Qiandongnan Vocational and Technical College for Nationalities, Kaili 556000, China

ARTICLE INFO

ABSTRACT

Epimedium total flavonoid capsules (ETFCs), a traditional Chinese patent medicine derived from *Epimedium brevicornu* Maxim., have been used for centuries to treat primary osteoporosis and are associated with kidney yang deficiency symptoms. Based on the "kidney-brain axis" hypothesis, previous study demonstrated that ETFCs can improve the cognitive function of MCAO rats, and the mechanism may involve the inflammatory response. However, little is known about their therapeutic components and scientific connotations. This study systematically investigates the anti-neuroinflammatory material basis and the mechanisms of ETFCs, integrating UPLC-Q/TOF-MS and UPLC-TQ-MS for chemical profiling, quantitative analysis of key components in rats' plasma and brain, along with network pharmacology and activity verification. As a result, 65 components were identified. Metabolite profiling showed a total of 130 xenobiotics, highlighting the extensive metabolic transformations. Pharmacokinetic studies showed that primary flavonoid glycosides were quickly absorbed, while secondary glycosides exhibited slower absorption and elimination. In brain tissue, both prototype glycosides and secondary glycosides reached their peak concentrations rapidly, with T_{max} between 0.25–1 h, while the prototype glycosides were eliminated after 8 h and secondary glycosides exhibited a secondary peak at 6–8 h. A network pharmacology study revealed that prototypes in blood may play a therapeutic role through targets including AKR1B1, PDE5A, and PTGS2 (COX-2). The LPS-induced BV-2 cell model confirmed ETFCs' constituents showed inhibitory activities on pro-inflammatory cytokine secretion, mRNA expressions of IL-6, TNF-α, COX-2, iNOS and could down-regulate the protein expressions of COX-2 and iNOS. This research lays the foundation for the further development and utilization of ETFCs.

1. Introduction

Epimedium brevicornu Maxim., also known as Yin Yang Huo or Horny Goat Weed, is a Yang-enhancing and kidney-nourishing herb with a long history in traditional Chinese medicine (TCM) (Chen et al., 2015; Jiang et al., 2015; Ma et al., 2011). According to TCM theory, "the kidneys produce marrow, and the marrow nourishes the brain", emphasizing the close relationship between kidneys and the brain (Feng et al., 2021). Therefore, the guiding principle of TCM in treating cognitive decline or neurological disorders is to tonify the kidneys, thus nourishing the

* Corresponding authors at: State Key Laboratory on Technologies for Chinese Medicine Pharmaceutical Process Control and Intelligent Manufacture, Jiangsu Kanion Pharmaceutical Co. Ltd., Jiangsu, Lianyungang, 222001, China.
** Corresponding author.
E-mail addresses: lihaibo1985124@sina.com (H. Li), xwv8521@kanion.com (W. Xiao), 1018yuyang@jnu.edu.cn (Y. Yu).
[1] The first two authors contributed equally to this work.

marrow to enhance brain function.

Studies have shown that *E. brevicornu* is rich in isopentenyl flavanones, which exert a tonifying effect on the kidneys (Chen et al., 2015; Qian et al., 2024; Zhang et al., 2016). Numerous literature reports highlight the use of *E. brevicornu* in the treatment of neurological disorders, ischemic stroke, and other conditions, especially regarding its potential to enhance cognitive abilities by tonifying the kidneys (Lin et al., 2013; Wu et al., 2023; Xie et al., 2022; Xu et al., 2022). Epimedium total flavonoid capsule (ETFC), derived from the extraction of *E. brevicornu*, is a categorized Chinese patent medicine developed by Jiangsu Kangyuan Pharmaceutical Co., Ltd. and approved by the National Medical Products Administration. It is clinically used for primary osteoporosis associated with kidney yang deficiency syndrome,

characterized by symptoms such as lower back pain, cold feet, frequent nocturia, and a pale tongue with a thin white coating. Extensive clinical applications have confirmed the safety and efficacy of ETFCs (Lu et al., 2013). In addition, a variety of bioactive compounds in *Epimedium*, especially flavonoids, have been the focus of research on chronic diseases such as tonifying the kidneys, strengthening bones, and improving cognitive ability (Jin et al., 2019; Li et al., 2015; Zhang et al., 2023).

It is well known that the therapeutic efficacy of orally administered TCM usually depends on the interaction between its active constituents and specific biological targets within the body. A comprehensive understanding of the serum pharmacokinetics of orally administered TCM is crucial for elucidating the absorption, distribution, metabolism, and excretion (ADME) of these active components (Li et al., 2022). In
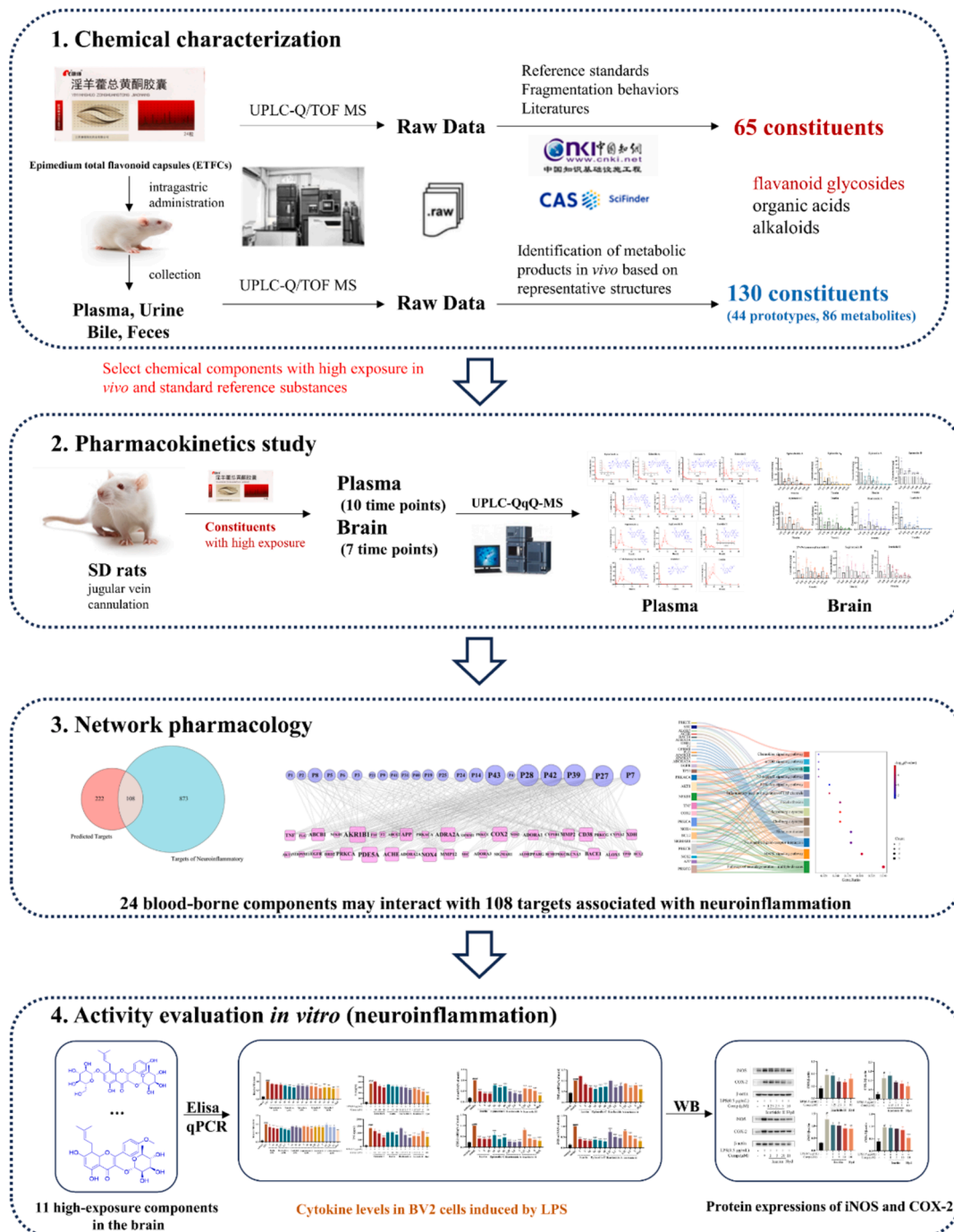

Fig. 1. Research strategy.

particular, considering the impact of the blood–brain barrier in neurological diseases, accounting for the temporal and spatial dynamics of components within target tissues will contribute to our understanding of the biological mechanisms underlying their efficacy. It is noteworthy that the characteristics of the mechanisms of action of TCM formulas are highly analogous to the holistic, systematic, and comprehensive nature of network pharmacology. Utilizing network pharmacology to explore the potential targets of TCM formulas, which are characterized by "multiple components," is currently a mainstream research approach (Qin et al., 2024; Xiang et al., 2024; Zhao et al., 2023).

Based on the speculation that *Epimedium* tonifies the kidneys and may benefit the brain, we conducted a preliminary study on the improvement of post-stroke cognitive impairment (PSCI) by ETFCs (Yang et al., 2024). The results showed that ETFCs could improve cognitive function in middle cerebral artery occlusion (MCAO) stroke model rats, potentially through regulating the expression of p-IκBα and p-NF-κB proteins, thereby inhibiting neuroinflammation. However, the *in vivo* therapeutic components and scientific connotation remain unclear. To address these, our ongoing study aims to investigate the anti-neuroinflammatory material basis as well as the underlying mechanisms of ETFCs at both *in vitro* and *in vivo* levels. Hence, a five-step method was employed, involving UPLC qualitative and quantitative analysis techniques coupled with the network pharmacological study and *in vitro* experimental validation (Fig. 1.). Firstly, the composition analysis of ETFCs was elucidated using UPLC-Q-TOF-MS technology; Secondly, we described the complex multi-component metabolic characteristics of orally administered ETFCs in rats, while simultaneously characterizing the *in vivo* pharmacokinetic properties of its main constituents in both blood and brain tissues. This step has revealed highly exposed components within target tissues that may be associated with pharmacological effects, providing a more comprehensive interpretation of the chemical basis underlying the ETFCs' efficacy. Furthermore, we used network pharmacology combined with experimental validation to reveal the effects and mechanisms of ETFCs in improving neuroinflammation. By elucidating its complex composition, pharmacokinetics, and molecular mechanisms of action, our findings pave the way for the development of ETFCs-based therapeutics for the management of PSCI and related neuroinflammatory disorders.

2. Materials and methods

2.1. Chemicals and reagents

ETFCs were obtained from Kanion Pharmaceutical Co., Ltd ((Lot No. 210603, Jiangsu, China). Sagittatoside A, sagittatoside B, 2″-O-rhamnosyl icariside, ikarisoside A, epimedoside A, chlorogenic acid and hyperoside were purchased from Chengdu Purifa Technology Co., Ltd. (Chengdu, China). Icariin, epimedin A$_1$, epimedin A, epimedin C, icariside I, icariside II and icaritin were purchased from Chengdu Herbpurify Co., Ltd. (Chengdu, China). Neochlorogenic acid, magnoflorine, and epimedin B were purchased from Shanghai Winherb Medical Technology Co., Ltd. (Shanghai, China). Cryptochlorogenic acid was purchased from Chengdu Push Bio-technology Co., Ltd (Chengdu, China). The purity of each compound was more than 98 % determined by HPLC analysis. Detailed information on the standards used in this study is shown in Table S1.

LC-MS-grade acetonitrile and methanol were purchased from Fisher Scientific (Fairlawn, NJ, USA). LC-MS-grade formic acid was obtained from Sigma-Aldrich (St. Louis, MO, USA). Information on other materials can be found in corresponding methods.

2.2. Animal and administration of ETFCs

Male Sprague Dawley (SD) rats, each weighing 250 ± 10 g, were obtained from the Medical Experimental Animal Center of Guangdong Province. They were kept under controlled conditions: a constant temperature of 23 °C, humidity of 55 %, a 12-hour light–dark cycle, and free access to food and water. Prior to the experiment, all rats underwent a one-week acclimation period. All procedures and management of all experimental animals strictly followed the "The Provision and General Recommendation for the Chinese Experimental Animals Administration Legislation guidance" approved by the Science and Technology Department of Jiangsu Province (Ethical Review No. ky2023030311 and ky2023010512.).

In the metabolic study, 10 male SD rats were randomly assigned to either the ETFCs group (n = 6) or the blank group (n = 4). The ETFCs group received an intragastric dose of ETFCs at 667 mg/kg/day for three days, while the blank group was given normal saline following the same schedule.

In the pharmacokinetic study, 7 male SD rats underwent jugular vein cannulation and recovered 12 h before administration. Then the rats received an oral dose of ETFCs at 1.33 g/kg/day.

In the brain tissue distribution study, after one week of acclimatization feeding, 48 male SD rats (250 ± 20 g) were also given ETFCs orally at the same dosage of 1.33 g/kg/day.

2.3. Biological Samples' collection and pretreatment

2.3.1. For metabolic study

Plasma samples: Four rats were anesthetized with an intraperitoneal injection of 10 % chloral hydrate after the final dose. Blood from the hepatic portal vein was collected at 0.5, 1, 2, and 4 h. These plasma samples (500 μL each) were combined to create pooled plasma. Protein precipitation was performed by adding acetonitrile (three volumes) containing 0.1 % formic acid, followed by vortexing and centrifugation at 14,000 rpm for 10 min. The supernatant was then dried under nitrogen gas, and the residue was reconstituted in 200 μL of methanol.

Urine and feces samples: After ETFCs administration, urine and feces were collected over three days. Daily urine samples were pooled and centrifuged at 14,000 rpm for 10 min. The supernatant (10 mL) was applied to pre-activated SPE columns, washed with water, and eluted with methanol. The methanol eluent was dried under nitrogen at room temperature, and the residue was reconstituted in 200 μL methanol. Dried feces samples (1.0 g) were ground, soaked in 10 mL methanol for 24 h, and ultrasonically extracted for 60 min. The fecal extract was centrifuged at 14,000 rpm for 10 min, then the supernatant was evaporated to dryness and the residue re-dissolved in 5 mL water. This solution was processed on SPE columns similarly to the urine samples, with the final residue reconstituted in 500 μL methanol.

Bile samples: On the third-day post-administration, rats were anesthetized, and their bile ducts were cannulated using polyethylene tubing. A heating lamp was used to maintain body temperature. Bile (5 mL) was collected over 8 h and centrifuged at 14,000 rpm for 10 min. The supernatant was then processed using SPE columns following the same procedure as the urine samples. The final residue was reconstituted in 500 μL methanol.

Blank samples were processed identically. For analysis, 2 μL of plasma and urine samples and 1 μL of feces and bile samples were injected.

2.3.2. For quantitative study

Plasma: Blood samples were taken from the jugular vein at various time points (0.25, 0.5, 2, 4, 6, 8, 12, 24, 36, and 48 h) after ETFCs administration and placed in heparinized Eppendorf tubes. These were centrifuged at 14,000 rpm and 4 °C for 10 min to obtain plasma. Each 100 μL plasma sample was mixed with 50 μL methanol and 50 μL internal standard (isobavachin 10 ng/mL), followed by 300 μL acetonitrile (0.1 % formic acid) for protein precipitation. The mixture was vortexed for 2 min, centrifuged at 14,000 rpm for 10 min, then dried under nitrogen gas. The residue was reconstituted with 100 μL methanol, vortexed for 2 min, and centrifuged again at 14,000 rpm for 20 min. Finally, 2 μL of the supernatant was injected into UPLC-TQ/MS for analysis.

Brain tissue: After administration, the rats were anesthetized quickly and brain tissues were collected at 0.25, 0.5, 2, 4, 6, 8, and 12 h (n = 6 at each time point). The surface of the brain tissues was quickly washed with ice saline, dried with filter paper, and stored at $-80\,°C$ until analysis. The brain tissue was accurately weighed and homogenized with the four-fold volume of physiological saline to obtain a homogenate. 50 μL of methanol and 50 μL of IS were added to 100 μL of the homogenate. The subsequent steps were consistent with the procedures described for the treatment of plasma samples above.

2.4. UPLC-Q/TOF-MS

Chromatography analysis was performed using an Acquity UPLC I-Class system with a binary solvent system and an automatic sample manager. Separation occurred on a Waters BEH C_{18} column (2.1 mm × 100 mm, 1.7 μm) at 35 °C. The mobile phases were water (A) and acetonitrile (B), both with 0.1 % formic acid, delivered at 0.4 mL/min. The gradient program was: 0–2.5 min, 2–18 % B; 2.5–8.5 min, 18–31 % B; 8.5–11.5 min, 31–33 % B; 11.5–12.0 min, 33–50 % B; 12.0–13.5 min, 50–60 % B; 13.5–14.5 min, 60–100 % B; 14.5–15.0 min, 100 % B; 15–16 min, 100–2 % B; 16–17 min, 2 % B. The injection volume was 2 μL.

The UPLC system was coupled with a SYNAPTTM G2 HDMS quadrupole time-of-flight mass spectrometer (Waters, Manchester, U.K.), featuring an electrospray ionization (ESI) source. The settings were: capillary voltage of 3.0 kV (ESI$^+$) or -2.0 kV (ESI$^-$); sample cone voltage of 40 V (ESI$^+$) or 30 V (ESI$^-$); extraction cone voltage of 4 V; source temperature at 100 °C; desolvation temperature at 300 °C; cone gas flow at 50 L/h; and desolvation gas flow at 800 L/h. For mass accuracy in MSE mode, Sodium formate solution was used for calibration across 50–1500 Da, and Leucine-enkephalin (m/z 556.2771 in ESI$^+$ mode; m/z 554.2615 in ESI$^-$ mode) served as an external reference at a constant flow rate of 5 μL/min.

2.5. UPLC-QqQ-MS

Components separation was achieved using an Acquity^{TM} UPLC I-Class system (Waters Corp., Milford, MA, USA). Detailed information on chromatography analysis was given in Supplementary Material S1.2.

The UPLC system was paired with a Xevo TQ-XS mass spectrometer (Waters Corp., Milford, MA, USA) featuring an electrospray ionization (ESI) source. Multiple Reaction Monitoring (MRM) parameters for quantitative and semi-quantitative analytes in the pharmacokinetics and brain tissue study are optimized and shown in Table S2 and S3.

2.6. Method validation of pharmacokinetic research

In adherence to the 2018 FDA guidelines for bioanalytical method validation, a comprehensive assessment was conducted, encompassing specificity, linear response, sensitivity thresholds, as well as metrics for precision and accuracy. The extraction efficiency, matrix interference, and analyte stability were also rigorously evaluated. A detailed exposition of the validation procedures is delineated in Supplementary Material S1.3.

2.7. Network pharmacology

2.7.1. Target collection

The molecular structures of 23 bioavailable compounds in plasma, formatted in SMILES, were submitted to the SwissTargetPrediction platform (https://www.swisstargetprediction.ch/) for target prediction specific to 'Homo sapiens' (Gfeller et al., 2014). This initiative aimed to identify potential interactions between these compounds and pertinent protein targets. Concurrently, a targeted search within the CTD database (https://ctdbase.org/) was conducted, leveraging the keyword 'neuroinflammation' to extract genes associated with neuroinflammatory

conditions. By mapping these gene names to their corresponding Uni-Prot IDs, a comprehensive, non-redundant set of 330 neuroinflammatory-related target genes was compiled. Subsequently, the targets with a "Relevance score" greater than the mediator value were identified as neuroinflammation targets. The targets of 23 compounds for the treatment of neuroinflammation were obtained by overlaying the neuroinflammation targets with the predicted targets of these compounds. Ultimately, the compound-target network was built and the key target was extracted based on the mediator values of degree.

2.7.2. Enrichment analysis

All key targets were obtained from 2.7.1 and subsequently used for the enrichment analysis of Gene Ontology (GO) annotation and Kyoto Encyclopedia of Genes and Genomes (KEGG) pathways. GO annotation and KEGG pathways analysis were conducted using the DAVID Bioinformatics Resources (https://david.ncifcrf.gov/), focusing on genes significantly associated with the study. The terms of PB, CC, MF and KEGG were obtained through a conditional screen that simultaneously satisfied 5 genes and a confidence level of 0.05. This analysis aimed to dissect the KEGG pathways linked to neuroinflammation, providing a visual representation of their interconnectedness and relevance.

2.7.3. Molecular docking

In order to verify the binding affinity between the active compound and targets, molecular docking was employed with the 5 highest-degree targets in the compound-target network to 23 bioavailable compounds. All molecular docking was performed using Autodock software. The target structures were extracted from the PDB database, which containing small molecule-target complexes, and their grid centers were determined based on the positions of the small molecules in the complexes. The grid size was 20 × 20 × 20. The 23 bioavailable compounds were prepared including hydrogenation and energy minimization.

2.8. In vitro anti-neuroinflammatory activity evaluation of potential bioactive components

2.8.1. Cell culture and treatment

The BV-2 murine microglial cell line was cultivated in DMEM (Gibco, USA) with 10 % fetal bovine serum (ExCell Bio, China) 100 IU/mL penicillin, and 100 μg/mL streptomycin. The cells were maintained in a controlled atmosphere of 37 °C and 5 % CO2, ensuring a humidified environment for optimal growth.

2.8.2. CCK8 assay

BV-2 cells were seeded into 96-well plates at 5×10^4 cells per mL (100 μL per well) overnight, and then the medium was discarded and 100 μL medium containing components were added to each well. Following a 24-hour exposure, 10 μL of the CCK8 reagent (GLPBIO, China) was introduced into each well for a subsequent 2-hour incubation period. Subsequently, the optical density was determined at a wavelength of 450 nm. Each trial was conducted three times to ensure reproducibility.

2.8.3. NO assay

Nitric oxide (NO) production, reflected by nitrite levels in the culture supernatant, was assessed using the Griess reaction. BV-2 cells were plated in a 96-well format at a concentration of 1.3×10^4 cells/mL for an initial 24-hour period, with 100 μL of medium per well. Subsequently, the growth medium was aspirated and replaced with 100 μL of fresh medium containing 0.5 μg/mL LPS (Sigma-Aldrich, USA) along with varying doses of the test compounds, followed by a 24-hour incubation. The assay was concluded by combining 50 μL of the supernatant with an equal volume of Griess reagent (Beyotime Biotechnology Co., Ltd, China), after which the optical density was recorded at 540 nm. The nitrite levels were then extrapolated from a sodium nitrite standard curve.

2.8.4. Elisa and quantitative PCR

Utilizing a protocol congruent with the procedures outlined for the "NO assay", cells were subjected to treatment. Post-treatment, supernatants were harvested for the quantification of interleukin-6 (IL-6) and tumor necrosis factor-alpha (TNF-α) using enzyme-linked immunosorbent assay (ELISA) kits procured from 4A Biotech Co., Ltd, China. The assays were executed in strict accordance with the guidelines provided by the manufacturer.

BV-2 cells' total RNA was harvested utilizing Servicebio's extraction kit, following the manufacturer's recommended protocol. Subsequently, 1 μg RNA was converted to cDNA by using SweScript All-in-One SuperMix and gDNA Remover according to the reaction system in the instructions (Servicebio, China). Finally, the intended DNA bands were amplified with 10 μL SYBR Green qPCR Master Mix (Servicebio, China), 0.4 μL primers, and 2 μL cDNA. The sequences of PCR primers used are listed in Table S15.

2.8.5. Western blot

After LPS induction and drug treatment for 24 h, BV-2 cells were collected and lysed with RIPA buffer (Thermo Fisher, USA). The supernatant was obtained by high-speed centrifugation, followed by total protein quantification analysis using the BCA protein assay kit (Beyotime Biotechnology Co., Ltd, China). Protein samples, each weighing 40 μg, were resolved on a 10 % SDS-PAGE gel and subsequently transferred to a PVDF membrane. Post-transfer, the membranes were saturated with a 5 % non-fat milk solution for 2 h at ambient temperature prior to an overnight incubation with primary antibodies at 4 °C. Following three rounds of washing with TBST, the membranes were exposed to secondary antibodies for 2 h at room temperature. The immunoreactive bands were detected using an ECL detection kit from Absin and their intensities were measured employing the Image J software.

3. Results

3.1. Identification of EFTC-related prototypes in rats' bio-samples

The base peak intensity (BPI) chromatograms of ETFCs in positive and negative ion modes are shown in Fig. 2. The results showed that 65 chemical components were detected in ETFCs (Fig. S1, Table S4), including 54 flavonoids (41 isopentenyl flavanones), 8 organic acids, 1 alkaloid, and 2 other types. Among them, 16 chromatographic peaks were accurately identified by comparison with the reference standards. Based on the analysis of chemical composition, it can be observed that isopentenyl flavanones are the main ingredients of ETFCs. The detailed analysis of the compounds can be found in the Supplementary Material S2.

Based on the chemical profile of ETFCs, characteristic mass patterns of ingredients were used for the identification of prototypes. Utilizing retention times and mass spectrometry data, 44 distinct prototypes were identified following oral ingestion of ETFCs. Of these, Detection across biological matrices revealed the presence of 24 prototypes in plasma, 25 in urine, 30 in bile, and 33 in fecal matter, as detailed in Fig. 3A and Table 1. Notably, the plasma-exposed prototypes were predominantly isopentenyl flavanone glycosides, suggesting their candidacy as bioactive constituents, as depicted in Fig. 4.

3.2. Identification of EFTC-related metabolites in rats' bio-samples

The analysis strategy of "homologous metabolites identification based on representative structures" was employed to quickly identify related metabolites in rats following oral administration of ETFCs (Geng et al., 2014). Three aglycones, kaempferol, quercetin, and icariin, were defined as representative structures and imported into Metabolynx XS software. Using MDF technology, potential metabolites in rats' biological samples were screened. As a result, a total of 86 metabolites were characterized, including 16 metabolites in plasma, 41 in urine, 43 in bile, and 37 in feces (Fig. 3B, Table 2). There were few metabolites found in plasma, primarily glucuronidation products of secondary glycosides
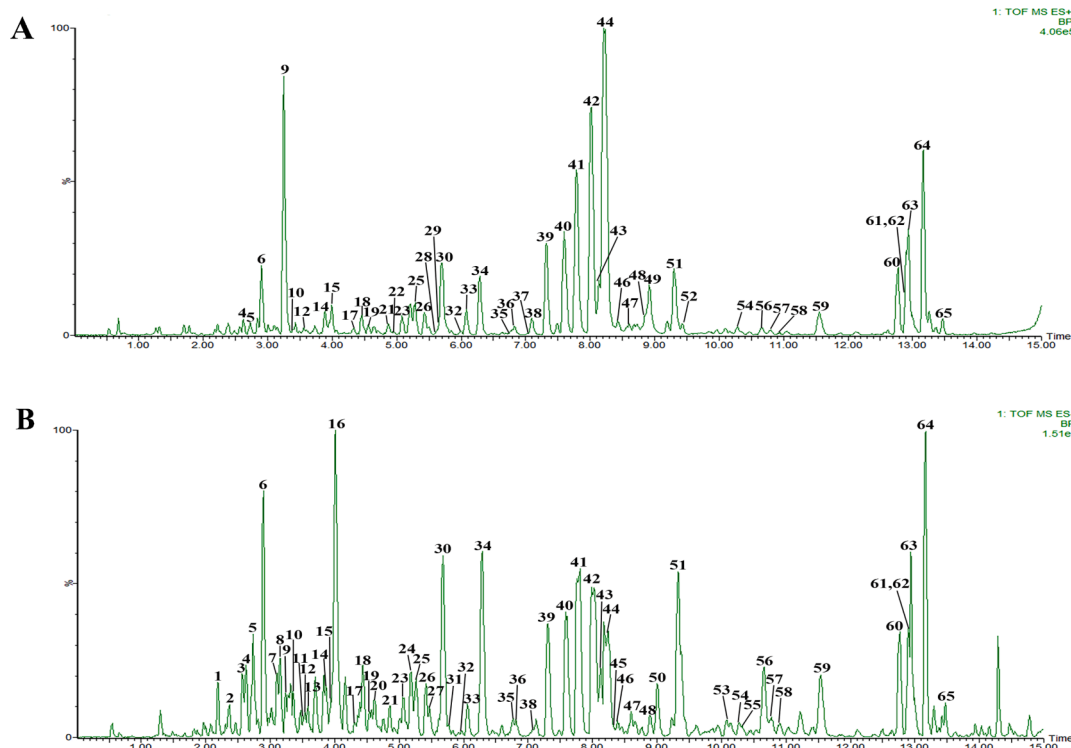

Fig. 2. The base peak intensity (BPI) chromatograms of ETFCs. (A) (+) ESI-MS chromatogram of ETFCs. (B) (−) ESI-MS chromatogram of ETFCs.
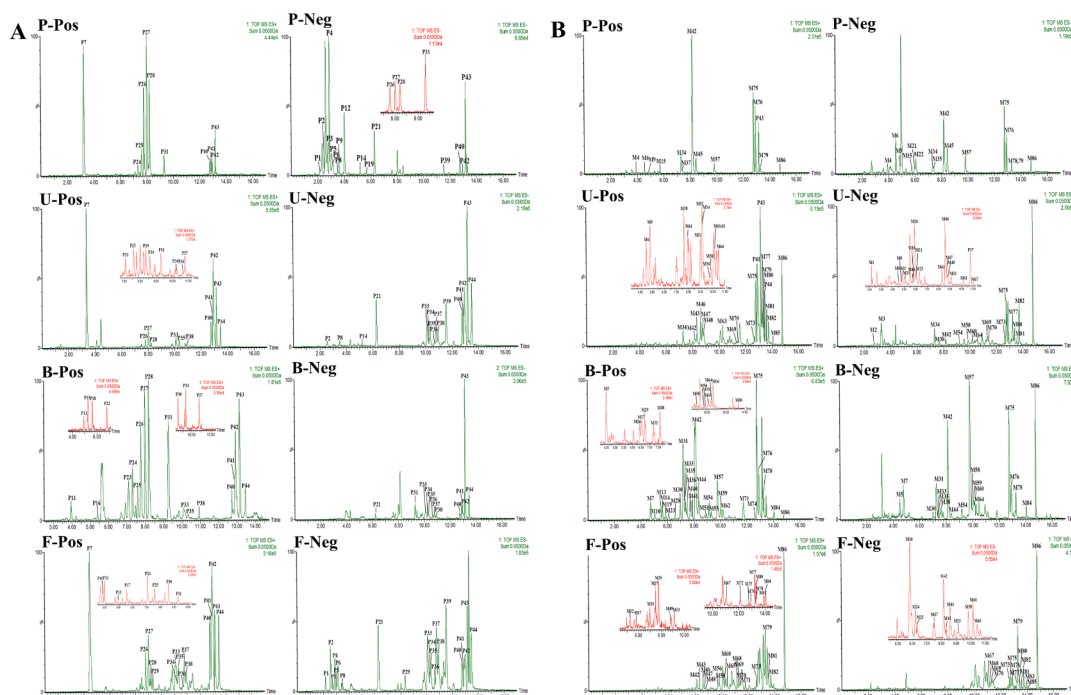
Fig. 3. Extracted ion chromatograms (EICs) of xenobiotics after oral administration of ETFCs. (A) EICs of ETFCs related prototypes and (B) EICs of ETFCs related metabolites in rats. (P, U, B, and F represented rat plasma, urine, bile and fecal samples; Pos and Neg meant positive and negative ion modes).

and aglycones, and their responses were higher than those of the prototypes of isopentenyl flavanones glycosides. The detailed analysis of the compounds can be found in the Supplementary Material S3.

3.3. Method validation of pharmacokinetic research

Based on the metabolic study of ETFCs in rats, 11 isopentenyl flavanone glycosides, including epimedoside A, epimedin A$_1$, epimedin A, epimedin B, epimedin C, icariin, ikarisoside A, sagittatoside A, sagittatoside B, 2″-O-rhamnosyl icariside and icariside, which were detected in rat plasma, showing high exposure levels with available reference substances. Furthermore, compounds such as icariside I and icaritin, identifiable in urine samples, are documented for their bioactivity (Bi et al., 2022; Zhang et al., 2023). Therefore, the above 13 compounds were selected as the quantitative components of plasma pharmacokinetics, with 11 being absorbable into the brain tissue. The method validation was carried out according to FDA bioanalytical method validation guidelines with the following results:

Plasma-specificity testing confirmed the absence of interference from endogenous substances at the analytes' and internal standard's (IS) retention times, as illustrated in Fig. S3. The plasma's quantitative constituents demonstrated a robust linear correlation (R^2 > 0.99) across the specified linear range detailed in Table S5. The LLOQs for plasma analytes spanned a range from 0.03 to 0.25 ng/mL, ensuring precision and accuracy aligned with the stipulated analytical criteria, as noted in Table S6. As displayed in Table S7, the intra-day and inter-day precision (RSD%) of three concentrations in plasma ranged between 1.71 % and 9.93 %. Concurrently, the RE% for accuracy was confined within a range from −4.25 % to 5.02 %. The matrix effects of the 13 quantitative components and IS in plasma at three concentrations were between 85.49 % and 106.94 % with RSDs within 8.79 %. Consistently, the recovery rates for the aforementioned analytes ranged between 80.66 % and 100.44 %, with icariside I showing a slightly lower range of 62.79 % to 69.80 %. The RSDs for these recoveries were contained within an 11.74 % margin, as summarized in Table S8. The stability test data of the 13 analytes under four different conditions are shown in Table S9. Their RSDs ranged from −4.01 % to 14.08 %, and accuracy was less than

14.60 %. Moreover, this method ensured no residual interference from the 13 compounds in plasma (Fig. S4).

Above all, the validated method can be applied to the pharmacokinetic analysis of the 13 components in rat plasma. Similarly, full method validation in rat brain tissue demonstrated good specificity, linearity, accuracy, precision, matrix effect, extraction recovery, and stability for 11 components. The results are summarized in Fig. S5-S6 and Table S10–S14.

3.4. Pharmacokinetic studies

3.4.1. Plasma

The optimized approach was successfully applied to simultaneously measure 13 key components in rat plasma after oral administration of ETFCs. The mean plasma concentration–time profile and corresponding pharmacokinetic parameters are displayed in Fig. 5 and Table 3, respectively. According to the metabolic profile, the plasma metabolites of isopentenyl flavone glucosides primarily existed in the form of glucuronidation. The dynamic changes in the metabolites together with the prototypes contributed to describing the overall dynamic characteristics of ETFCs *in vivo*. Therefore, the pharmacokinetic characteristics of 8 semi-quantitative components were also monitored by using peak area-time change curves (Fig. S7).

The pharmacokinetic profiles of the 13 ingredients revealed that the mean plasma concentration–time curves for 6 prototype glycosides (epimedoside A, epimedin A$_1$, epimedin A$_1$, epimedin B, epimedin C, and icariin) exhibited a consistent trend. These glycosides were rapidly absorbed (T_{max} < 1h) and quickly eliminated *in vivo*, with a short mean residence time (MRT). Additionally, the prototype glycosides exhibited a small maximum plasma concentration (C$_{max}$). Their poor absorption in plasma is likely due to the difficulty in transporting through intestinal epithelial cells and initial hydrolysis in the intestines, converting them into secondary glycosides (Chen et al., 2011; Zhou et al., 2013).

Compared with prototype glycosides, the secondary glycosides and aglycones (sagittatoside A, sagittatoside B, 2″-O-rhamnosyl icariside, icariside, and icaritin) displayed distinct pharmacokinetic characteristics. Their pharmacokinetic profiles exhibited two peaks, and the MRT

Table 1

UPLC-Q-TOF/MS data of the prototypes of ETFCs in rat biological samples.

No	t_R	Elemental composition	Selected ion	Measured mass	Calculated mass	Mass error	MS/MS or MS^E fragmentation		Identification	Source
							ESI$^+$	ESI$^-$		
P1	2.18	$C_{16}H_{18}O_9$	[M−H]$^-$	353.0876	353.0873	0.8	N/A	191.0525, 179.0354, 135.0457	neochlorogenic acid	P F
P2	2.56	$C_{16}H_{18}O_8$	[M−H]$^-$	337.0923	337.0923	0.9	N/A	191.0556, 163.0404	*trans*-5-*O*-*p*-coumaroylquinic acid	P U F
P3	2.73	$C_{16}H_{18}O_9$	[M−H]$^-$	353.0870	353.0873	−0.8	N/A	191.0493, 179.0345	chlorogenic acid	P F
P4	2.89	$C_9H_6O_4$	[M−H]$^-$	177.0191	177.0188	0.3	N/A	133.0298	5,7-dihydroxychromone	P F
P5	3.09	$C_{16}H_{18}O_8$	[M−H]$^-$	337.0914	337.0923	−0.9	N/A	191.0562, 163.0434	4-*O*-*p*-coumaroylquinic acid	P F
P6	3.15	$C_{16}H_{18}O_8$	[M−H]$^-$	337.0922	337.0923	−0.3	N/A	191.0544, 163.0391	3-*O*-*p*-coumaroylquinic acid	P F
P7	3.26	$C_{20}H_{23}NO_4$	[M + H]$^+$	342.1708	342.1705	0.9	297.1135, 282.0866, 265.0872, 237.0906, 191.0857	N/A	magnoflorine	P U F
P8	3.52	$C_{16}H_{18}O_8$	[M−H]$^-$	337.0928	337.0923	1.5	N/A	191.0558, 163.0390	*cis*-5-*O*-*p*-coumaroylquinic acid	P U F
P9	3.59	$C_9H_8O_3$	[M−H]$^-$	163.0402	163.0395	4.3	N/A	119.0501	*p*-hydroxycinnamic acid	P
P10	3.90	$C_{21}H_{20}O_{12}$	[M + H]$^+$	465.1041	465.1033	1.7	303.0511, 287.0555, 177.0915	N/A	hyperoside	F
P11	3.97	$C_{27}H_{30}O_{14}$	[M + H]$^+$	579.1715	579.1714	0.2	N/A	431.0986, 285.0422	kaempferol-3,7-di-*O*-rhamnoside	F B
P12	4.03	$C_{18}H_{24}O_{10}$	[M−H]$^-$	399.1284	399.1291	−1.8	N/A	237.0762, 219.0658, 193.0860	unknow	P
P13	4.93	$C_{33}H_{42}O_{17}$	[M + H]$^+$	711.2486	711.2500	−2.1	565.1931, 403.1412, 385.1279	N/A	unknow	F B
P14	5.19	$C_{20}H_{18}O_{10}$	[M−H]$^-$	417.0820	417.0822	−0.5	N/A	285.0396	kaempferol-3-*O*-xylopyranoside	P U
P15	5.26	$C_{38}H_{48}O_{20}$	[M + H]$^+$	825.2800	825.2817	−2.1	663.2275, 517.1714, 355.2614	N/A	diphylloside A	B
P16	5.43	$C_{37}H_{46}O_{19}$	[M + H]$^+$	795.2681	795.2712	−3.9	663.2304, 517.1724, 355.1189	N/A	epimedoside E	B
P17	5.60	$C_{39}H_{52}O_{20}$	[M + H]$^+$	841.3121	841.3130	−1.1	695.2548, 549.1592, 387.1438, 369.1323	N/A	icariside D	F
P18	5.62	$C_{33}H_{42}O_{16}$	[M + H]$^+$	695.2550	695.2551	−0.1	549.1975, 387.1433, 369.1323, 313.0713	N/A	icariside B	B
P19	5.68	$C_{32}H_{38}O_{15}$	[M−H]$^-$	661.2132	661.2132	0.0	N/A	514.1442, 499.1745, 353.0998	epimedoside A	P
P20	5.76	$C_{38}H_{48}O_{19}$	[M + H]$^+$	809.2850	809.2868	−2.2	663.2325, 517.1689, 355.185	N/A	diphylloside B	B
P21	6.29	$C_{24}H_{34}O_9$	[M−H]$^-$	465.2129	465.2125	0.5	N/A	303.1598, 285.1509	taxifolin-7-*O*-glucoside	P U F B
P22	6.82	$C_{39}H_{48}O_{20}$	[M + H]$^+$	837.2816	837.2817	−0.1	705.2366, 367.1174, 355.1172	N/A	4''-*O*-acetyl-3-*O*-xylopyranosyl epimedoside A	B
P23	7.09	$C_{28}H_{32}O_{14}$	[M + H]$^+$	593.1872	593.187	0.3	447.1274, 285.0766	N/A	acacetin 7-*O*-rutinoside	U F B
P24	7.31	$C_{39}H_{50}O_{20}$	[M + H]$^+$	839.2973	839.2974	−0.1	677.2449, 531.1893, 369.1347, 313.0722	N/A	epimedin A$_1$	P B
P25	7.60	$C_{39}H_{50}O_{20}$	[M + H]$^+$	839.2953	839.2974	−2.5	677.2421, 531.1862, 369.1336, 313.0714	N/A	epimedin A	P U F B
P26	7.77	$C_{38}H_{48}O_{19}$	[M + H]$^+$	809.2847	809.2868	−2.6	677.2443, 531.1856, 369.1323, 313.0710	645.2172, 512.2684, 366.1107, 351.0872	epimedin B	P U F B

Table 1 (*continued*)

No	t_R	Elemental composition	Selected ion	Measured mass	Calculated mass	Mass error	MS/MS or MS^E fragmentation		Identification	Source
							ESI$^+$	ESI$^-$		
P27	8.01	$C_{39}H_{50}O_{19}$	$[M+H]^+$	823.3006	823.3025	−2.3	677.2428, 531.1854, 369.1337, 313.0706	659.2327, 366.1097, 351.0867	epimedin C	P U F B
P28	8.21	$C_{33}H_{40}O_{15}$	$[M+H]^+$	677.2437	677.2445	−1.2	531.1866, 369.1333, 313.0709	513.1795, 367.1162, 352.0911, 297.0391	icariin	P U F B
P29	8.35	$C_{33}H_{42}O_{15}$	$[M-H]^-$	677.2462	677.2445	2.5	N/A	384.1214, 367.1151, 341.1018	wanepimedoside A	U F
P30	8.60	$C_{27}H_{32}O_{11}$	$[M+H]^+$	533.2021	533.2023	−0.4	387.1446, 369.1335, 313.0715	N/A	4′-methoxynoricaritin-3-O-rhamnoside	U F B
P31	9.28	$C_{39}H_{48}O_{19}$	$[M+H]^+$	821.288	821.2868	1.5	677.2415, 531.1870, 369.1317, 313.0717	529.1692, 367.1181	icaritin-3-O-(2-hydroxy-2-carboxyl-5-methyltetrahydrofuran-1-yl) rhamnopyranoside-7-O-glucopyranoside	P U F B
P32	9.41	$C_{40}H_{50}O_{20}$	$[M+H]^+$	851.2985	851.2974	−1.9	719.2525, 531.1849, 369.1320	N/A	sempervirenoside B	B
P33	10.09	$C_{32}H_{38}O_{15}$	$[M-H]^-$	661.2135	661.2132	0.5	355.1183, 299.0562	353.1014, 297.0405	ikarisoside B or its isomer	U F B
P34	10.28	$C_{27}H_{30}O_{11}$	$[M-H]^-$	529.1704	529.1710	−1.5	385.1288, 369.2430	383.1128, 297.0397	caohuoside C or its isomer	U F B
P35	10.32	$C_{32}H_{38}O_{15}$	$[M-H]^-$	661.2136	661.2132	0.6	355.1178, 299.0551	353.1019	ikarisoside B or its isomer	U F B
P36	10.64	$C_{27}H_{30}O_{11}$	$[M-H]^-$	529.1697	529.1710	−2.5	N/A	383.1099, 297.0391	caohuoside C or its isomer	U F B
P37	10.78	$C_{31}H_{36}O_{14}$	$[M-H]^-$	631.2022	631.2027	−0.8	355.1185, 299.0555	353.1003	ikarisoside F	U F B
P38	10.92	$C_{32}H_{38}O_{14}$	$[M-H]^-$	645.2188	645.2183	0.8	501.1762, 355.1181, 299.0557	352.0953	2′-O-rhamnosyl ikarisoside A	U F B
P39	11.54	$C_{26}H_{28}O_{10}$	$[M-H]^-$	499.1612	499.1604	1.6	N/A	353.1023, 309.0399, 281.0459	ikarisoside A	P U F
P40	12.76	$C_{33}H_{40}O_{15}$	$[M+H]^+$	677.2441	677.2445	−0.6	369.1337, 313.0712	531.2291, 367.1180, 352.0931, 298.0481	sagittatoside A	P U F B
P41	12.90	$C_{32}H_{38}O_{14}$	$[M+H]^+$	647.2332	647.2340	−1.2	369.1344, 313.0719	366.1101, 351.0886, 323.0907	sagittatoside B	P U F B
P42	12.93	$C_{33}H_{40}O_{14}$	$[M+H]^+$	661.2495	661.2496	−0.2	369.1340, 313.0716	366.1104, 351.0870, 323.0919	2″-O-rhamnosyl icariside II	P U F B
P43	13.17	$C_{27}H_{30}O_{10}$	$[M+H]^+$	515.1910	515.1917	−1.4	369.1333, 313.0710	366.1107, 351.0865, 323.0920	icariside II	P U F B
P44	13.46	$C_{33}H_{38}O_{14}$	$[M-H]^-$	657.2186	657.2183	0.5	515.1936, 369.1349, 313.0717	513.1763, 367.1185, 352.0951	3‴-carbonyl-2′-β-L-quinovosyl icariside II	U F B

Note: P, U, B and F represents plasma, urine, bile, and feces; N/A: not detected.

values were obviously prolonged compared to prototype glycosides. Among them, icariside II had a T_{max} value of 0.29 ± 0.10 h, differing from other secondary glycosides, as monoglycosides can pass through the intestinal epithelium more quickly than oligoglycosides and aglycones (Fokialakis et al., 2019).
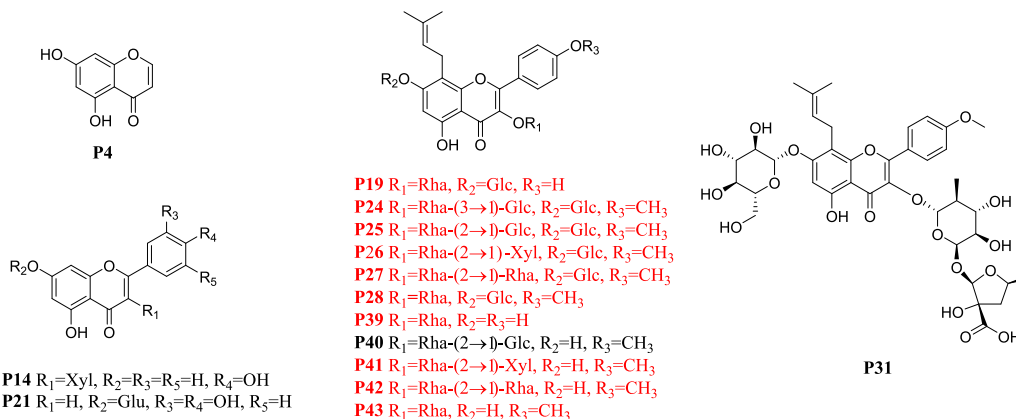
The results of pharmacokinetic parameters showed that icariin, icariside II, and epimedin C had higher exposure levels than others in plasma, with their AUC_{0-t} (ng*h/mL) values at 28.63 ± 5.79, 22.98 ± 17.55, and 23.48 ± 11.27, respectively. Although the initial glycoside forms and their subsequent derivatives had modest areas under the AUC and C_{max} values, the glucuronide conjugates exhibited greater bioavailability and a more prolonged elimination phase.
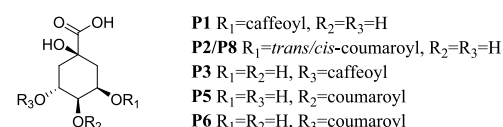
3.4.2. Brain tissue

According to the pharmacokinetics of TCM, only those prototypes or related metabolites that reach effective concentrations and exposure times in blood and target tissues may be the potential bioactive components (Wang, 2002). Considering the influence of the blood–brain barrier in neurological diseases, studying the dynamic changes of components in brain tissue can help identify the effective components of EFTCs. Consequently, a method for the simultaneous determination of 11 prototypes absorbed in brain tissue was established and applied to study the concentration–time changes after ETFCs administration. As depicted in Fig. 6 and Table 4, icariin showed the maximum AUC value, followed by icariside II and epimedin C, with values of 35.36 ± 5.56, 33.29 ± 6.32, and 28.53 ± 4.51 ng*h/mL, respectively. The quantitative ingredients reached maximum concentration rapidly with T_{max} values between 0.25–1 h, indicating that isopentenyl flavanones can rapidly distribute through the blood–brain barrier to reach the target tissue. Among them, the prototype glycosides were basically eliminated after
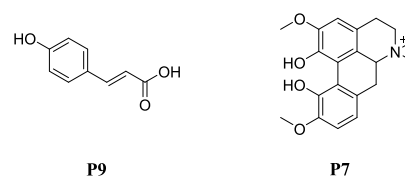
Flavonoids

P4

P19 R$_1$=Rha, R$_2$=Glc, R$_3$=H
P24 R$_1$=Rha-(3→l)-Glc, R$_2$=Glc, R$_3$=CH$_3$
P25 R$_1$=Rha-(2→l)-Glc, R$_2$=Glc, R$_3$=CH$_3$
P26 R$_1$=Rha-(2→1)-Xyl, R$_2$=Glc, R$_3$=CH$_3$
P27 R$_1$=Rha-(2→l)-Rha, R$_2$=Glc, R$_3$=CH$_3$
P28 R$_1$=Rha, R$_2$=Glc, R$_3$=CH$_3$
P39 R$_1$=Rha, R$_2$=R$_3$=H
P40 R$_1$=Rha-(2→l)-Glc, R$_2$=H, R$_3$=CH$_3$
P41 R$_1$=Rha-(2→l)-Xyl, R$_2$=H, R$_3$=CH$_3$
P42 R$_1$=Rha-(2→l)-Rha, R$_2$=H, R$_3$=CH$_3$
P43 R$_1$=Rha, R$_2$=H, R$_3$=CH$_3$

P31

P14 R$_1$=Xyl, R$_2$=R$_3$=R$_5$=H, R$_4$=OH
P21 R$_1$=H, R$_2$=Glu, R$_3$=R$_4$=OH, R$_5$=H

Organic acids

P1 R$_1$=caffeoyl, R$_2$=R$_3$=H
P2/P8 R$_1$=*trans/cis*-coumaroyl, R$_2$=R$_3$=H
P3 R$_1$=R$_2$=H, R$_3$=caffeoyl
P5 R$_1$=R$_3$=H, R$_2$=coumaroyl
P6 R$_1$=R$_2$=H, R$_3$=coumaroyl

P9

Alkaloids

P7

The components marked in red can be detected in the brain tissue

Fig. 4. Chemical structures of the prototypes absorbed in plasma after oral administration of ETFCs.

8h, but secondary glycosides had a secondary peak at 8 h, likely due to the transformation of prototype glycosides.

In addition, we compared the contents of quantitative ingredients in ETFC extract (Xu et al., 2018) with their exposure in plasma and brain tissue. The results revealed that the abundance of icariside II in ETFC extract was much lower than icariin and epimedin C, but their exposure in blood and brain tissue was comparable. The exposure characteristics of prototypes in rat plasma and brain tissue were generally similar. For example, icariin, icariside II, and epimedin C exhibited significant exposure in both plasma and brain tissue, suggesting that they were crucial for the pharmacological effects of ETFCs. The above findings provide a basis for selecting representative components for subsequent *in vitro* activity evaluations.

3.5. Network pharmacology

A target prediction using the SwissTargetPrediction database revealed that 24 compounds acted on 330 targets. A further 981 neuroinflammation-related protein targets were extracted from the GenCard database. A total of 108 target duplications were identified in the context of neuroinflammation-related targets and compound targets of action (Fig. 7A), indicating that the 24 compounds acted on 108 neuroinflammation-related targets. Subsequently, a compound-target interaction network was constructed, comprising 132 nodes and 385 edges. In this network, 22 compounds and 44 targets exhibited degree values equal to or greater than the mediator value (4) (Fig. 7B and Table S16). Among these, compounds P28, P39, and P42, which had the highest degree values, may represent promising therapeutic agents for neuroinflammation. Similarly, AKR1B1, PDE5A PTGS2 (COX-2), ADRA2A, and ACHE, which also had the highest degree values, may represent promising key targets for the therapeutic effects of these compounds on neuroinflammation and were used for molecular docking (Table S17). A KEGG pathway analysis of 44 key targets revealed that these targets were primarily focused on neuroinflammation disease-related pathways, including MAPK signaling pathway, neuroactive ligand-receptor interaction, and NF-κB signaling pathway pathways

(Fig. 7C) (Shabab et al., 2017; Vezzani et al., 2019). To gain further insight into the potential of these compounds for treating neuroinflammation, we conducted a more detailed examination of their impact on inflammatory factors.

The results of molecular docking indicated that the binding affinities between the 5 highest-degree targets in the compound-target network and the 23 bioavailable compounds were better than −5.8 kcal/mol (Fig. S8), which suggested the presence of a robust interaction between the small molecule and the target (Li et al., 2020a). Among these targets, COX-2 played a primary role in neuroinflammation and thus became a focus target. In consideration of the docking scoring and the accessibility of the small molecules, only compounds P27, P28, P39, P42 and P43 were subjected to testing for their inhibitory activity against COX-2.

3.6. Anti-neuroinflammatory activity evaluation of the potential active components in ETFCs

Microglial cells play a critical role in regulating neuronal activity, promoting learning, and shaping social behavior. When activated, microglia release various inflammatory mediators that can lead to neuroinflammation (Guruswamy and ElAli, 2017; Woodburn et al., 2021). Given their crucial regulatory role in the central nervous system, inhibiting their activation is key to alleviating neuroinflammation and achieving neuroprotection. The LPS-induced BV-2 cell model is often employed as an *in vitro* model for anti-neuroinflammatory studies. Based on the quantitative results of plasma and brain tissue, combined with the results of compounds-targets interaction network analysis, 11 ingredients were selected for *in vitro* anti-neuroinflammatory activity evaluation. First, the maximum non-toxic concentration of each compound was determined (Fig. S9). The results shown in Fig. 8A demonstrated that all 11 compounds could significantly inhibit NO production, exhibiting significant anti-neuroinflammatory activity.

Additionally, based on the exposure levels of the 11 compounds in plasma and brain tissue, as well as their structural characteristics, we selected icariin, icariside II, epimedin C, and ikarisoside A as representative compounds to further verify their anti-neuroinflammatory effects.

Table 2
UPLC-Q-TOF/MS data of the metabolites of ETFCs in rat biological samples.

No	t_R	Elemental composition	Selected ion	Measured mass	Calculated mass	Mass error	MS/MS or MS^E fragmentation ESI$^+$	ESI$^-$	Identification	Source
M1	2.16	$C_{10}H_{12}O_4$	[M−H]$^-$	195.0664	195.0657	3.6	N/A	150.0321	methyl-hydrocaffeic acid	U
M2	2.76	$C_{17}H_{20}O_9$	[M−H]$^-$	367.1033	367.1029	1.1	N/A	191.0347	(trans or cis) 4-O-methylcaffeoylquinic acid	U
M3	3.34	$C_{17}H_{20}O_9$	[M−H]$^-$	367.1024	367.1029	−1.4	N/A	191.0562, 173.0461	(trans or cis) 4-O-methylcaffeoylquinic acid	U
M4	3.92	$C_{21}H_{18}O_{13}$	[M + H]$^+$	479.0836	479.0826	2.1	303.0507	301.0339	quercetin + GluA	P
M5	4.48	$C_{21}H_{18}O_{12}$	[M + H]$^+$	463.0873	463.0877	−0.9	287.0551	285.0401	kaempferol + GluA	B
M6	4.55	$C_{21}H_{18}O_{12}$	[M + H]$^+$	463.0874	463.0877	−0.6	287.0557	285.0401	kaempferol + GluA	P U
M7	4.72	$C_{32}H_{34}O_{18}$	[M + H]$^+$	707.1824	707.1823	0.1	531.1509, 355.1189, 299.0563	529.1342, 353.1029	icaritin − CH_2 + 2GluA	B
M8	4.83	$C_{22}H_{20}O_{13}$	[M−H]$^-$	491.0815	491.0826	−2.2	N/A	315.0500, 300.0281	quercetin + CH_2 + GluA	U
M9	4.87	$C_{21}H_{18}O_{12}$	[M + H]$^+$	463.0886	463.0877	1.9	287.0561	285.0403	kaempferol + GluA	P U
M10	5.04	$C_{33}H_{38}O_{17}$	[M + H]$^+$	707.2167	707.2187	−6.9	561.1601, 543.1605, 385.1623, 367.1179	N/A	icariside II + GluA + O	B
M11	5.08	$C_{22}H_{20}O_{13}$	[M−H]$^-$	491.0825	491.0826	−0.2	N/A	315.0502	quercetin + CH_2 + GluA	U
M12	5.27	$C_{39}H_{52}O_{21}$	[M + H]$^+$	857.3047	857.3079	−3.7	711.2467, 565.1907, 403.1392, 385.1279, 313.0721	N/A	epimedin C + O + H_2O	F
M13	5.49	$C_{32}H_{36}O_{16}$	[M + H]$^+$	677.2085	677.2082	0.4	531.1508, 355.1188, 299.0565	N/A	icariside II − CH_2 + GluA	B
M14	5.62	$C_{38}H_{48}O_{19}$	[M + H]$^+$	809.2866	809.2868	−0.2	663.2283, 517.1714, 355.1187	N/A	epimedin C − CH_3	B
M15	5.74	$C_{26}H_{28}O_{12}$	[M + H]$^+$	533.1655	533.1659	−0.8	357.1341	355.1165, 327.1225,193.0857	icaritin − H_2 − CH_2 + GluA	P
M16	5.79	$C_{22}H_{20}O_{13}$	[M−H]$^-$	491.0824	491.0826	−0.4	N/A	315.0503, 300.0269	quercetin + CH_2 + GluA	U
M17	5.79	$C_{39}H_{50}O_{20}$	[M + H]$^+$	839.2935	839.2974	−4.6	693.2343, 547.1782, 385.1283, 367.1186	N/A	epimedin C + O	F
M18	5.89	$C_{15}H_{10}O_9S$	[M−H]$^-$	364.9975	364.9967	2.2	N/A	285.0400	kaempferol + sul	U F
M19	5.89	$C_{33}H_{38}O_{17}$	[M + H]$^+$	707.2172	707.2187	−2.1	561.1619, 385.1288	N/A	icariside II + GluA + O	B
M20	5.92	$C_{15}H_{10}O_{10}S$	[M−H]$^-$	380.9918	380.9916	0.8	N/A	301.0352, 151.0038	quercetin + sul	U
M21	5.95	$C_{15}H_{10}O_9S$	[M−H]$^-$	364.9968	364.9967	0.3	N/A	285.0394	kaempferol + sul	P U
M22	6.06	$C_{15}H_{10}O_9S$	[M−H]$^-$	364.997	364.9967	0.8	N/A	285.0410	kaempferol + sul	P
M23	6.08	$C_{32}H_{34}O_{18}$	[M + H]$^+$	707.1814	707.1823	−1.3	531.1501, 355.1182, 299.0557	N/A	icaritin − CH_2 + 2GluA	B
M24	6.2	$C_{16}H_{12}O_{10}S$	[M−H]$^-$	395.0087	395.0073	3.5	N/A	315.0508, 300.0273	quercetin + CH_2 + sul	F
M25	6.34	$C_{16}H_{12}O_{10}S$	[M−H]$^-$	395.0072	395.0073	−0.3	N/A	315.0506, 300.0273	quercetin + CH_2 + sul	U F
M26	6.43	$C_{26}H_{28}O_{13}$	[M + H]$^+$	549.1614	549.1608	1.1	373.1277, 355.1180	N/A	icaritin − CH_2 + GluA + H_2O	B
M27	6.50	$C_{26}H_{26}O_{13}$	[M + H]$^+$	547.145	547.1452	−0.4	371.1123, 353.2486	N/A	icaritin − CH_2 + GluA + O	B
M28	6.59	$C_{33}H_{38}O_{17}$	[M + H]$^+$	707.217	707.2187	−2.4	561.1602, 385.1299, 367.1187	N/A	icariside II + GluA + O	B
M29	6.72	$C_{26}H_{26}O_{13}$	[M + H]$^+$	547.1451	547.1452	−0.2	371.1137, 353.2484	N/A	icaritin − CH_2 + GluA + O	B
M30	6.98	$C_{39}H_{48}O_{21}$	[M + H]$^+$	853.2761	853.2766	−0.6	545.1674, 369.1338, 313.0722	675.2269, 513.2712, 367.1186	sagittatoside A + GluA	B F
M31	7.21	$C_{33}H_{36}O_{18}$	[M + H]$^+$	721.1982	721.198	0.3	545.1682, 369.1342, 313.0722	N/A	icaritin + 2GluA	B
M32	7.23	$C_{39}H_{46}O_{22}$	[M + H]$^+$	867.2551	867.2559	−0.9	545.1666, 369.1349, 313.0718	N/A	icariside II + 2GluA	B
M33	7.30	$C_{39}H_{48}O_{21}$	[M + H]$^+$	853.2759	853.2766	−0.8	545.1666, 369.1342, 313.0715	N/A	sagittatoside A + GluA	B
M34	7.32	$C_{33}H_{36}O_{18}$	[M + H]$^+$	721.1982	721.1980	0.3	545.1682, 369.1342, 313.0722	543.1509, 367.1184	icaritin + 2GluA	P U
M35	7.36	$C_{33}H_{38}O_{17}$	[M + H]$^+$	707.2181	707.2187	−0.8	531.1863, 369.1348, 313.0718	N/A	icaritin + glu + GluA	B P
M36	7.45	$C_{33}H_{38}O_{17}$	[M + H]$^+$	707.2173	707.2187	−2.0	545.1650, 369.1341, 313.0719	N/A	Icaritin + glu + GluA	B
M37	7.5	$C_{32}H_{40}O_{16}$	[M + H]$^+$	681.2375	681.2395	−2.9	549.1976, 403.1393, 385.1288, 369.1333	547.2902, 400.1168, 367.1184	sagittatoside B + O + H_2O	F
M38	7.64	$C_{27}H_{30}O_{13}$	[M + H]$^+$	563.1761	563.1765	−0.7	387.1434, 369.1335, 313.0715	385.1271, 367.1181	icaritin + H_2O + GluA	B U
M39	7.76	$C_{33}H_{42}O_{16}$	[M + H]$^+$	695.2537	695.2551	−2.0	549.1976, 531.1846, 387.1111, 369.1333	N/A	icariin + H_2O	F
M40	7.72	$C_{38}H_{46}O_{20}$	[M + H]$^+$	823.2659	823.2661	−0.2	691.2255, 545.1655, 369.1334	N/A	sagittatoside B + GluA	B
M41	7.96	$C_{39}H_{48}O_{20}$	[M + H]$^+$	837.2803	837.2817	−1.7	691.2224, 545.1657, 369.1335, 313.0713	N/A	2″-O-rhamnosyl icariside III + GluA	U B
M42	8.16	$C_{33}H_{38}O_{16}$	[M + H]$^+$	691.2222	691.2238	−2.3	545.1655, 369.1341, 313.0776	513.1759, 366.1098	icariside II + GluA	P U F B
M43	8.29	$C_{15}H_{10}O_5$	[M−H]$^-$	269.0463	269.045	4.8	N/A	N/A	kaempferol − O	U F
M44	8.39	$C_{26}H_{26}O_{12}$	[M + H]$^+$	531.1497	531.1503	−1.1	355.1177, 299.0551	353.10332, 298.0484	icaritin − CH_2 + GluA	B
M45	8.44	$C_{26}H_{26}O_{12}$	[M + H]$^+$	531.1503	531.1503	0.0	355.1175, 299.0559	353.10332, 298.0484	icaritin − CH_2 + GluA	P
M46	8.59	$C_{15}H_{10}O_6$	[M−H]$^-$	285.0402	285.0399	1.1	N/A	N/A	qercetin − O	U F
M47	8.73	$C_{16}H_{12}O_6$	[M−H]$^-$	299.0562	299.0556	2	286.0473	285.1492, 284.0329	kaempferol + CH_2	U F
M48	8.81	$C_{16}H_{12}O_6$	[M−H]$^-$	299.056	299.0556	1.3	286.0472	285.1499, 284.0334	kaempferol + CH_2	U F

(continued on next page)

Table 2 (*continued*)

No	t_R	Elemental composition	Selected ion	Measured mass	Calculated mass	Mass error	MS/MS or MS^E fragmentation ESI$^+$	ESI$^-$	Identification	Source
M49	8.81	$C_{38}H_{46}O_{20}$	$[M+H]^+$	823.2682	823.2661	2.6	677.2120, 531.1875, 355.2682	N/A	2″-O-rhamnosyl icariside II − CH_2 + GluA	F
M50	8.91	$C_{27}H_{30}O_{11}$	$[M+H]^+$	531.1863	531.1866	−0.6	385.1292, 367.1186	N/A	icariside II + O	B
M51	8.94	$C_{27}H_{28}O_{13}$	$[M+H]^+$	561.1616	561.1608	1.4	545.1667, 385.1297, 367.1195	N/A	icaritin + GluA + O	B U
M52	9.12	$C_{16}H_{12}O_7$	$[M-H]^-$	315.0515	315.0505	3.2	302.0436	300.0286	quercetin + CH_2	U
M53	9.12	$C_{32}H_{38}O_{16}$	$[M+H]^+$	679.2238	679.2238	0.0	661.2437, 531.1865, 481.2814, 371.1136, 315.0499	N/A	icariin − CH_3 + O	F
M54	9.15	$C_{27}H_{28}O_{13}$	$[M+H]^+$	561.1612	561.1608	0.7	385.1293, 367.1187, 313.0719	N/A	icaritin + O + GluA	B U
M55	9.32	$C_{27}H_{28}O_{13}$	$[M+H]^+$	561.1601	561.1608	−1.2	385.2181, 369.1327	N/A	icaritin + O + GluA	B
M56	9.74	$C_{32}H_{38}O_{15}$	$[M+H]^+$	663.2292	663.2298	0.5	385.1296, 367.1189, 313.0716	N/A	sagittatoside B + O	F B U
M57	9.77	$C_{26}H_{26}O_{12}$	$[M+H]^+$	531.1520	531.1503	3.2	355.1179, 299.0555	353.1013	icaritin − CH_2 + GluA	P B
M58	9.85	$C_{33}H_{40}O_{15}$	$[M+H]^+$	677.2438	677.2445	−1.0	659.2379, 531.1879, 385.1279, 367.1191	N/A	2″-O-rhamnosyl icariside II + O	B F U
M59	10.04	$C_{27}H_{28}O_{13}$	$[M+H]^+$	561.1605	561.1608	−0.5	385.1288, 367.1194, 355.2643, 313.0716	383.1132, 352.0946	icaritin + GluA + O	B
M60	10.16	$C_{33}H_{40}O_{15}$	$[M+H]^+$	677.2433	677.2445	−1.8	659.2323, 531.1873, 385.1290, 367.1190	N/A	2″-O-rhamnosyl icariside II + O	B F U
M61	10.18	$C_{17}H_{12}O_8$	$[M-H]^-$	343.0461	343.0454	2	N/A	300.1655	quercetin + acetylation	U
M62	10.18	$C_{33}H_{36}O_{18}$	$[M+H]^+$	721.1965	721.198	−2.1	545.1653, 369.1333, 313.0713	N/A	icaritin + 2GluA	B
M63	10.26	$C_{33}H_{36}O_{18}$	$[M+H]^+$	721.1968	721.198	−1.7	545.1675, 369.1335, 313.0715	N/A	icaritin + 2GluA	U
M64	10.43	$C_{27}H_{30}O_{13}$	$[M+H]^+$	563.1761	563.1765	−0.7	545.1624, 387.1442, 369.1337, 313.0715	385.1283, 331.1911, 311.0556	icaritin + GluA + H_2O	B U
M65	10.45	$C_{33}H_{40}O_{16}$	$[M+H]^+$	693.2390	693.2395	−0.7	531.1875, 385.1286, 367.1190	N/A	icariin + O	F
M66	10.66	$C_{33}H_{36}O_{16}$	$[M+H]^+$	689.2075	689.2082	−1.0	543.1508, 513.1772, 367.1180	N/A	icarisdie II + GluA − H_2	B
M67	11.00	$C_{31}H_{36}O_{14}$	$[M+H]^+$	633.2181	633.2183	−0.3	355.1181	353.1031	sagittatoside B − CH_2	U F
M68	11.17	$C_{32}H_{38}O_{15}$	$[M+H]^+$	663.2282	663.2289	−1.1	531.1855, 385.1286	383.1115, 367.0804	sagittatoside B + O	F
M69	11.32	$C_{32}H_{38}O_{14}$	$[M+H]^+$	647.2318	647.234	−3.4	501.1751, 355.1180, 299.0552	352.0952	2″-O-rhamnosyl icariside II − CH_2	U F
M70	11.42	$C_{33}H_{40}O_{15}$	$[M+H]^+$	677.2435	677.2445	−1.5	531.1852, 385.1278	N/A	2″-O-rhamnosyl icariside II + O	U F
M71	11.73	$C_{33}H_{38}O_{16}$	$[M+H]^+$	691.2229	691.2238	−1.3	545.1658, 369.1340, 313.0717	N/A	icarisdie II + GluA	B F
M72	12.13	$C_{27}H_{30}O_{11}$	$[M+H]^+$	531.1868	531.1866	0.4	385.129	N/A	icariside II + O	F
M73	12.65	$C_{33}H_{38}O_{15}$	$[M+H]^+$	675.2285	675.2289	−0.6	543.1872, 355.1189, 299.0569	N/A	desmethylicaritin 3-O-rha (Ac)-xyl	U F
M74	12.73	$C_{33}H_{38}O_{16}$	$[M+H]^+$	691.2220	691.2238	−2.6	545.1658, 369.1341, 313.0714	N/A	icarisdie II + GluA	B
M75	12.77	$C_{27}H_{28}O_{12}$	$[M+H]^+$	545.1663	545.1659	0.7	369.1336, 313.0708	367.1179, 352.0948	icaritin + GluA	P U F B
M76	12.91	$C_{27}H_{28}O_{12}$	$[M+H]^+$	545.1666	545.1659	1.3	369.1344, 13.0715	367.1183, 352.0942	icaritin + GluA	P F B
M77	13.24	$C_{21}H_{22}O_7$	$[M+H]^+$	387.1443	387.1444	−0.3	369.1343, 313.0716	N/A	icaritin + H_2O	F U
M78	13.26	$C_{27}H_{28}O_{12}$	$[M+H]^+$	545.1660	545.1659	0.2	369.1338, 313.0719	367.1190, 352.0947	icaritin + GluA	P F B
M79	13.30	$C_{20}H_{18}O_6$	$[M+H]^+$	355.1180	355.1182	−0.6	299.0555	283.2636	icaritin − CH_2	P U F
M80	13.32	$C_{34}H_{40}O_{15}$	$[M+H]^+$	689.2429	689.2445	−2.3	369.1330, 299.0556, 313.0719	515.3051, 453.2318, 353.1035	anhydroicaritin 3-O-rha(Ac)-xyl	F U
M81	13.54	$C_{21}H_{20}O_7$	$[M+H]^+$	385.1280	385.1287	−1.8	367.1176, 313.0705	365.1118	icaritin + O	U F
M82	13.73	$C_{21}H_{20}O_7$	$[M+H]^+$	385.1287	385.1287	0.0	367.1188, 313.0721	365.1101, 337.2049	icaritin + O	U F
M83	13.93	$C_{30}H_{32}O_{12}$	$[M+H]^+$	585.1979	585.1972	1.2	369.1336, 313.0714	367.1177, 352.0936	anhydroicaritin-3-O-xyl (2Ac)	F
M84	14.05	$C_{21}H_{18}O_6$	$[M+H]^+$	367.1190	367.1182	2.2	313.1561	350.0764	icartin − H_2	B
M85	14.06	$C_{21}H_{18}O_7$	$[M+H]^+$	383.1119	383.1131	−3.1	365.1014, 313.0708	N/A	icartin − H_2 + O	U F
M86	14.77	$C_{21}H_{20}O_6$	$[M+H]^+$	369.1342	369.1338	1.1	313.0710	N/A	icaritin	P U F B

Note: P, U, B and F represents plasma, urine, bile, and feces; N/A: not detected.

The results from Elisa and qPCR experiments indicated that these four compounds could inhibit the secretion of the pro-inflammatory cytokines IL-6 and TNF-α, as well as the mRNA expressions of COX-2, iNOS, IL-6, and TNF-α (Fig. 8B-C). Specifically, icariside II and icariin dose-dependently reduced the protein expression levels of iNOS and COX-2 (Fig. 8D). These findings further support the role of these active ingredients in contributing to the efficacy of ETFCs.

4. Discussion

Stroke is a leading cause of mortality and long-term disability worldwide, with devastating consequences on both physical and cognitive functions (Kuriakose and Xiao, 2020; Li et al., 2020b). Among the complications that arise following a stroke, cognitive impairment stands out as a significant challenge, affecting patients' quality of life and posing a burden on healthcare systems (Kalaria et al., 2016; Mijajlović et al., 2017; Van Der Flier et al., 2018). Despite advancements in acute stroke management, there remains a critical need for effective
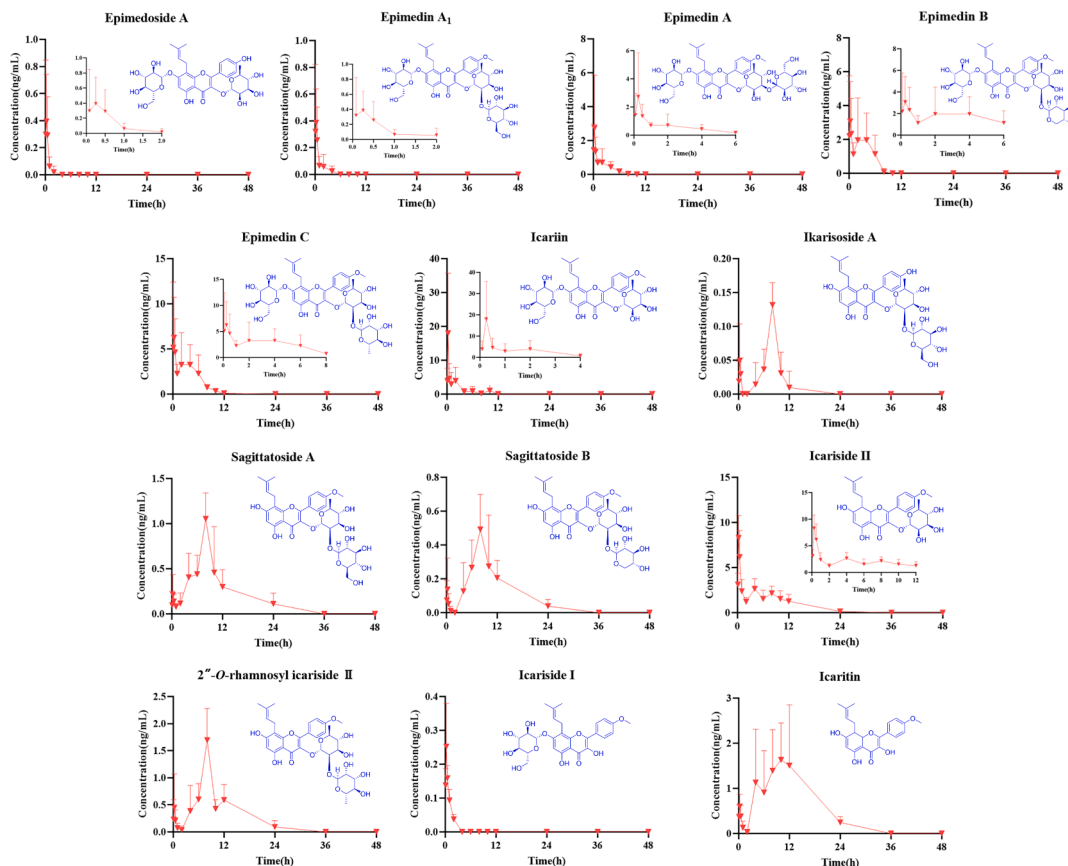
Fig. 5. Mean plasma concentration–time profiles of 13 components after oral administration of ETFCs (mean ± SD, n = 6).

Table 3
Pharmacokinetic parameters of 13 quantitative analytes in rat plasma after single oral administration of ETFCs (mean ± SD, n = 6).

Name	T_{max} (h)	$t_{1/2}$ (h)	C_{max} (ng/mL)	AUC_{0-t} (ng*h*mL^{-1})	$AUC_{0-\infty}$ (ng*h*mL^{-1})	MRT_{0-t} (h)	$MRT_{0-\infty}$ (h)
epimedoside A	1.22 ± 0.96	N/A	0.53 ± 0.18	0.41 ± 0.16	N/A	1.76 ± 0.83	N/A
epimedin A$_1$	0.26 ± 0.13	N/A	0.44 ± 0.38	0.37 ± 0.43	N/A	0.99 ± 0.89	N/A
epimedin A	0.26 ± 0.05	2.14 ± 0.36	2.83 ± 1.27	3.96 ± 0.96	4.41 ± 0.96	2.11 ± 0.38	2.92 ± 0.39
epimedin B	1.84 ± 1.03	1.01 ± 0.24	4.00 ± 1.10	11.17 ± 3.30	13.00 ± 4.90	2.97 ± 0.53	2.99 ± 0.73
epimedin C	1.80 ± 1.04	2.65 ± 1.03	8.00 ± 2.38	23.48 ± 4.60	24.68 ± 5.50	3.69 ± 0.35	4.45 ± 0.66
icariin	0.22 ± 0.02	16.11 ± 5.24	18.22 ± 7.16	22.98 ± 7.16	62.32 ± 21.59	2.68 ± 0.60	19.51 ± 8.17
ikarisoside A	7.67 ± 0.80	N/A	0.24 ± 0.08	0.66 ± 0.16	N/A	7.06 ± 0.27	N/A
sagittatoside A	7.67 ± 0.80	5.60 ± 0.65	1.14 ± 0.16	8.83 ± 1.23	9.14 ± 1.28	10.18 ± 0.96	10.94 ± 0.94
sagittatoside B	8.33 ± 0.33	13.75 ± 7.96	0.67 ± 0.14	4.52 ± 0.71	5.81 ± 1.33	10.04 ± 0.50	21.90 ± 10.67
icariside I	0.29 ± 0.04	0.80 ± 0.09	0.25 ± 0.05	0.22 ± 0.02	0.27 ± 0.02	0.70 ± 0.03	1.16 ± 0.14
icariside II	0.29 ± 0.04	12.72 ± 5.16	8.38 ± 0.98	28.63 ± 2.36	59.04 ± 22.26	6.24 ± 0.53	18.57 ± 7.64
icaritin	8.67 ± 1.12	5.64 ± 0.44	2.24 ± 0.43	22.79 ± 5.41	24.67 ± 5.34	10.73 ± 0.74	10.93 ± 0.69
2″-O-rhamnosyl icariside II	7.01 ± 1.42	7.54 ± 3.51	1.85 ± 0.34	12.31 ± 1.63	14.14 ± 2.29	9.53 ± 0.53	14.61 ± 4.82

therapeutic strategies targeting post-stroke cognitive impairment (PSCI) (Van Der Flier et al., 2018; Wu et al., 2019). ETFC is a Chinese patent medicine developed based on the TCM theory of "the kidney governing the bones". Considering the kidney-brain axis hypothesis, we are attempting to explore its indications for treating post-stroke cognitive impairment. In our previous study, an MCAO model was established to investigate cognitive impairments of ETFCs (Yang et al., 2024). The results suggested that ETFCs can effectively improve cognitive impairment and may act through the neuroinflammatory pathway. Therefore, to clarify the *in vivo* pharmacodynamic basis and mechanisms of ETFCs, this study focuses on neuroinflammation and analyzes the pharmacokinetics of ETFCs, as well as the quantification of exogenous components in target tissues. Through the integration of network pharmacology, potential pharmacodynamically active components were identified, followed by experimental validations against neuroinflammation. Our

findings provide scientific support for the mechanisms underlying the amelioration of PSCI by ETFCs through neuroinflammatory pathways.

In the treatment of nervous system diseases, the therapeutic effect of orally administrated TCM depends on whether its components can pass through the blood–brain barrier to reach the target organs. Some TCM components have sufficient bioavailability and brain tissue affinity, while many others struggle to reach the brain due to their chemical properties or molecular size, limiting their application in treating neurological diseases. The chemical composition of ETFCs was characterized by a complex array of flavone compounds, with poor absorption properties (Chen et al., 2008; Szabó et al., 2022). In view of the cognition-enhancing efficacy of ETFCs observed at the animal level, we further studied the blood circulation components of ETFCs and their plasma pharmacokinetics by using mass spectrometry. In particular, to address the question of whether the components reach the brain, a
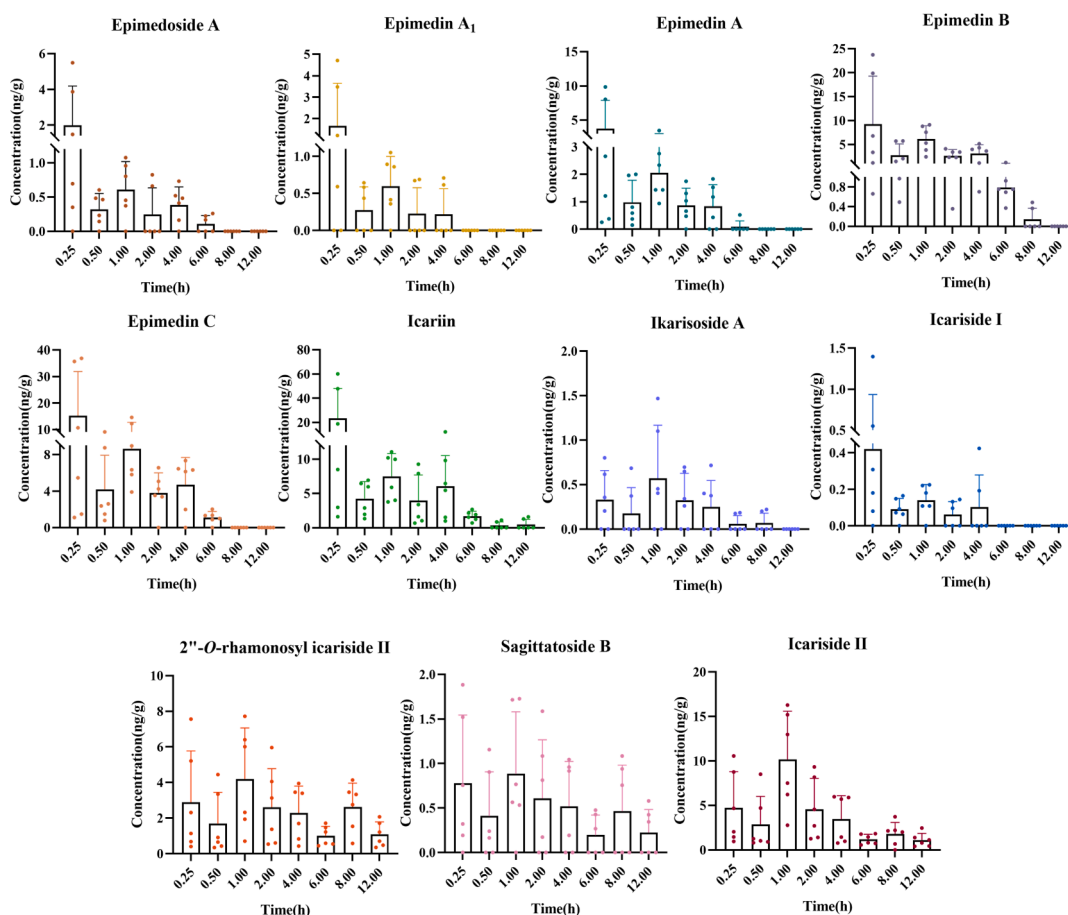
Fig. 6. Mean brain tissue concentration–time profiles of 11 components after oral administration of ETFCs (mean ± SD, n = 6).

Table 4
Pharmacokinetic parameters of 11 quantitative analytes in brain tissue after single oral administration of ETFCs (mean ± SD, n = 6).

Name	T_{max} (h)	$t_{1/2}$ (h)	C_{max} (ng/g)	AUC_{0-t} (ng*h*g^{-1})	$AUC_{0-\infty}$ (ng*h*g^{-1})	MRT_{0-t} (h)	$MRT_{0-\infty}$ (h)
epimedoside A	1.13 ± 0.59	3.63 ± 1.06	3.63 ± 1.06	2.68 ± 0.55	5.04 ± 0.73	1.85 ± 0.34	4.52 ± 1.00
epimedin A₁	1.13 ± 0.59	N/A	1.88 ± 0.72	1.70 ± 0.46	N/A	1.21 ± 0.30	N/A
epimedin A	1.25 ± 0.57	N/A	4.29 ± 1.51	5.02 ± 0.98	N/A	1.59 ± 0.36	N/A
epimedin B	1.25 ± 0.57	3.18 ± 1.11	10.68 ± 3.62	18.35 ± 2.92	20.69 ± 3.20	2.45 ± 0.27	4.27 ± 1.51
epimedin C	1.25 ± 0.57	2.30 ± 0.50	17.49 ± 6.04	28.53 ± 4.51	40.91 ± 1.80	2.07 ± 0.24	2.81 ± 1.60
icariin	1.13 ± 0.60	94.95 ± 77.71	25.50 ± 9.35	35.36 ± 5.56	286.79 ± 216.25	3.03 ± 0.57	94.95 ± 77.20
ikarisoside A	1.05 ± 0.28	N/A	0.88 ± 0.18	2.30 ± 0.66	N/A	2.28 ± 0.42	N/A
sagittatoside B	0.96 ± 0.12	10.43 ± 1.17	1.20 ± 0.28	5.75 ± 1.98	16.78 ± 0.99	3.21 ± 0.83	13.71 ± 1.69
icariside I	1.13 ± 0.59	N/A	0.49 ± 0.19	0.41 ± 0.15	N/A	1.15 ± 0.39	N/A
icariside II	1.04 ± 0.23	7.54 ± 1.71	9.53 ± 1.79	33.39 ± 6.32	44.71 ± 7.23	4.27 ± 0.22	10.07 ± 2.48
2″-O-rhamnosyl icariside II	2.13 ± 1.20	17.53 ± 9.35	4.85 ± 0.96	24.47 ± 4.59	64.96 ± 15.20	5.50 ± 0.33	24.15 ± 12.32

method was established for quantifying the content of components in brain tissue. Additionally, we described the temporal variation characteristics of the brain components at multiple time points. Thus, we have demonstrated that 11 key components of ETFCs can indeed enter brain tissue, thereby providing experimental support for its efficacy in improving cognitive function after stroke.

In network pharmacology study, we believe that it not only helps to reveal the multi-component and multi-target mechanisms of TCM but also provides significant support for the clinical application and pharmacological substance basis research (Shao and Zhang, 2013; Van Hasselt and Iyengar, 2019). The chemical composition of ETFCs is complex, comprising 65 identified components within the formula and over 130 exogenous substances detected in biological samples such as plasma. It is often difficult to evaluate and verify one by one by using traditional experimental methods, and it is even more challenging to

comprehensively understand its mechanism of action. Therefore, in this study, the network pharmacology technique was used to reveal the interaction network of multiple components and targets of ETFCs at the overall level and to identify its key active ingredients. A target prediction and network analysis identified 24 compounds acting on 108 neuroinflammation-related targets, highlighting key compounds (P28, P39, P42) and targets (AKR1B1, PDE5A, and PTGS2) involved in crucial neuroinflammation pathways. Based on previous animal experiments, the highly exposed components in brain tissue, as well as the structural representativeness of the components, we conducted experimental validation of 11 potential bioactive components in neuroinflammation pathways. The results showed that all 11 compounds could significantly inhibit the release of NO. Icariin, icariside II, epimedin C, and ikarisoside A were demonstrated to significantly reduce the secretion of inflammatory factors IL-6 and TNF-α, and inhibit their expression at the mRNA
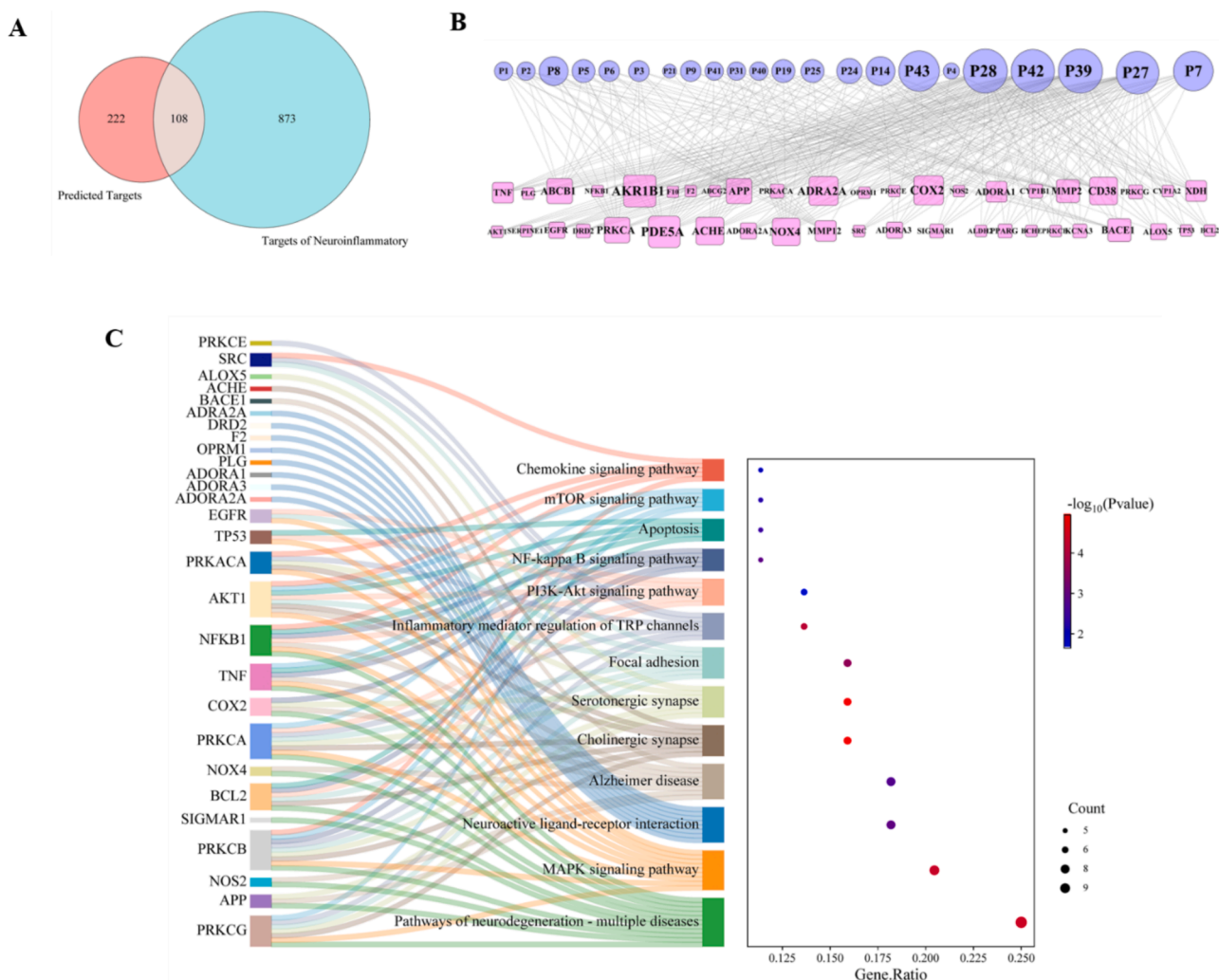
Fig. 7. (A) The Venn diagram illustrating the common gene targets of ETFCs and neuroinflammatory diseases. (B) The constructed compound-target interaction network. (C) Enriched KEGG pathways and their associated targets (via DAVID).

level, while also reducing the mRNA expressions of COX-2 and iNOS. Notably, icariin and icariside II, dose-dependently reduced iNOS protein expression. These results suggest that the structural diversity of iso-prenyl flavonoids in *E. brevicornu*, undergo complex and diverse meta-bolic reactions *in vivo*, transforming into corresponding secondary glycosides and metabolites to exert their effects. This provides important support for the new clinical application and pharmacological substance basis of ETFCs. This study acknowledges its limitations: it has thus far only evaluated the neuroinflammatory activity of 11 potential active ingredients *in vitro*. Future research should consider assessing a broader range of inflammatory markers and conducting further validation in animal models with larger sample sizes to enhance the generalizability of the findings. Moreover, the current investigation focused on the ac-tivity of individual compounds, neglecting the "multi-components" na-ture inherent in Traditional Chinese Medicine formulas. Subsequent studies should aim to explore the combined *in vivo* and *in vitro* neuro-inflammatory effects and mechanisms of these compound mixtures.

5. Conclusion

This study investigated the pharmacodynamic components of ETFCs against neuroinflammation through an integrated four-step strategy involving both *in vitro* and *in vivo* analyses. First, the metabolic profile of ETFCs was systematically characterized using UPLC-Q/TOF-MS, result-ing in the detection of a total of 130 xenobiotics (44 prototypes and 86

metabolites) in rat biological samples after oral administration of ETFCs. Second, two UPLC-TQ-MS/MS analytical methods were developed to describe the pharmacokinetic characteristics of the major absorbed components in rat plasma and brain tissue, respectively. Based on the quantitative data of plasma and brain tissue, combined with the network pharmacology analysis, 11 components with high exposure levels were screened out, potentially contributing to the anti-neuroinflammatory effect. Finally, the bioactivity evaluations provided the interpterion of the ETFCs's anti neuroinflammatory activities and mechanism. Conclusively, these findings provide a valuable reference for further research.

CRediT authorship contribution statement

Xiaochun Zeng: Writing – original draft, Methodology, Investiga-tion, Formal analysis, Data curation, Conceptualization. **Junran Shao:** Writing – original draft, Methodology, Investigation, Formal analysis, Data curation, Conceptualization. **Dabo Pan:** Software, Formal analysis, Data curation. **Siying Zeng:** Investigation, Formal analysis, Data cura-tion. **Zhenzhong Wang:** Supervision, Conceptualization. **Xinsheng Yao:** Software, Conceptualization. **Haibo Li:** Writing – review & editing, Supervision, Methodology, Investigation, Funding acquisition, Data curation, Conceptualization. **Wei Xiao:** Writing – review & editing, Supervision, Methodology, Investigation, Funding acquisition, Data curation, Conceptualization. **Yang Yu:** Writing – review & editing,
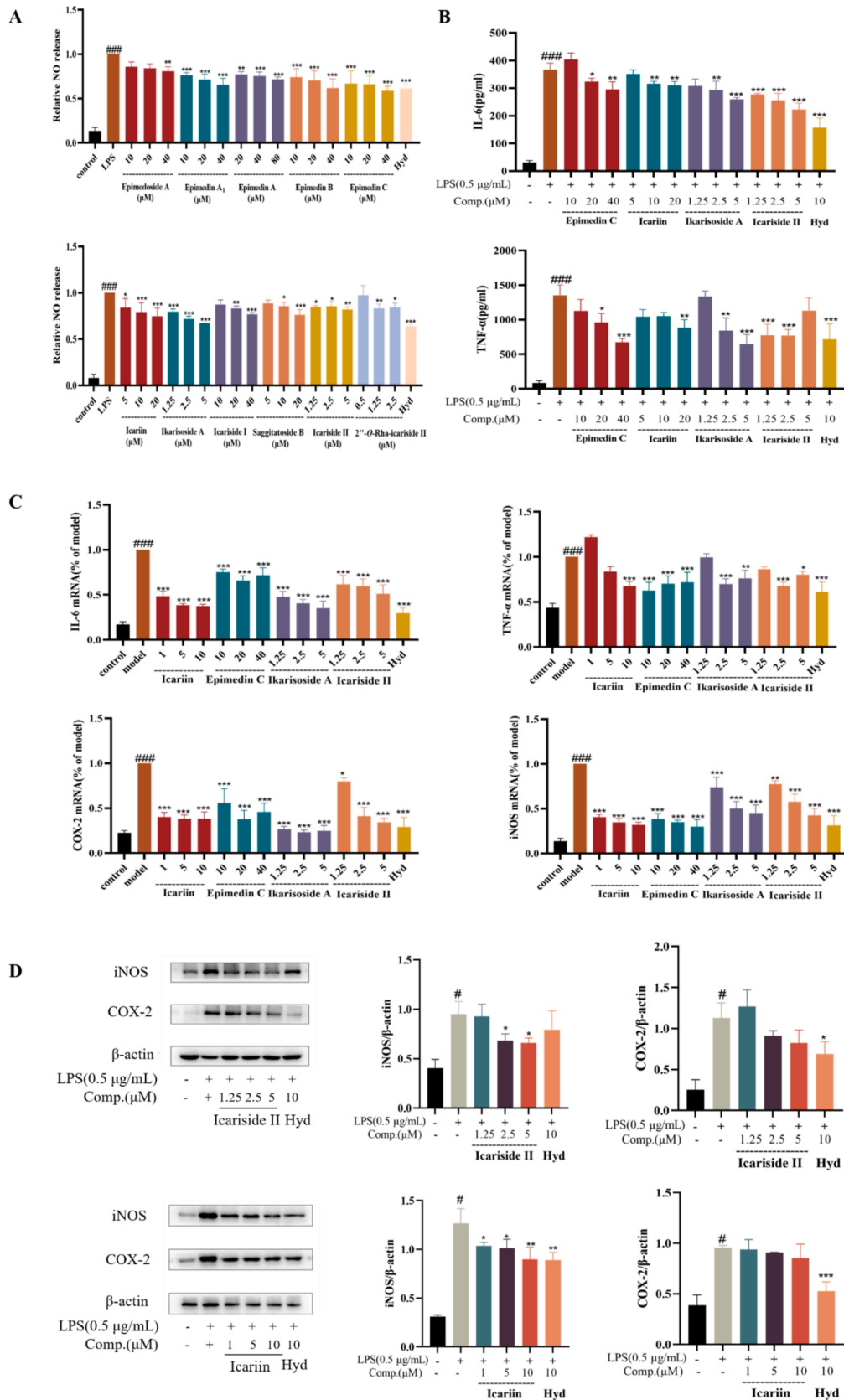
Fig. 8. (A) The production of NO in the supernatant. (B) The concentration of IL-6 and TNF-α in the supernatant. (C) Relative mRNA expressions of IL-6, COX-2, TNF-α, and iNOS. (D) The protein expressions of iNOS and COX-2. Data are mean ± SD (n = 3). *$P < 0.05$, **$P < 0.01$ vs. cells treated with LPS.

Methodology, Investigation, Funding acquisition, Data curation, Conceptualization.

Declaration of Competing Interest

The authors declare that they have no known competing financial interests or personal relationships that could have appeared to influence the work reported in this paper.

Acknowledgements

Appendix A. Supplementary data

Supplementary data to this article can be found online at https://doi.org/10.1016/j.arabjc.2024.106084.

References

Bi, Z.Y., Zhang, W., Yan, X.Y., 2022. Anti-inflammatory and immunoregulatory effects of icariin and icaritin. Biomed. Pharmacother. 151, 113180. https://doi.org/10.1016/j.biopha.2022.113180.

Chen, X.J., Tang, Z.H., Li, X.W., Xie, C.X., Lu, J.J., Wang, Y.T., 2015. Chemical constituents, quality control, and bioactivity of Epimedii Folium (Yinyanghuo). Am. J. Chin. Med. 43 (05), 783–834. https://doi.org/10.1142/S0192415X15500494.

Chen, Y., Zhao, Y.H., Jia, X.B., Hu, M., 2008. Intestinal absorption mechanisms of prenylated flavonoids present in the heat-processed Epimedium koreanum Nakai (Yin Yanghuo). Pharm. Res. 25 (9), 2190–2199. https://doi.org/10.1007/s11095-008-9602-7.

Chen, Y., Wang, J., Jia, X., Tan, X., Hu, M., 2011. Role of intestinal hydrolase in the absorption of prenylated flavonoids present in Yinyanghuo. Molecules 16 (2), 1336–1348. https://doi.org/10.3390/molecules16021336.

Feng, R., He, M.C., Li, Y., Wang, Y.J., Zhang, Y., 2021. Research progress on the regulation of kidney-tonifying Chinese herbs on brain based on theory of interaction between kidney and brain. Chin. J. Tradit. Chin. Med. 36 (04), 2179–2183.

Fokialakis, N., Alexi, X., Aligiannis, N., Boulaka, A., Meligova, A.K., Lambrinidis, G., Kalpoutzakis, E., Pratsinis, H., Cheilari, A., Mitsiou, D.J., Mitakou, S., Alexis, M.N., 2019. Biological evaluation of isoflavonoids from Genista halacsyi using estrogen-target cells: activities of glucosides compared to aglycones. PLoS One 14 (1), e0210247.

Geng, J.L., Dai, Y., Yao, Z.H., Qin, Z.F., Wang, X.L., Qin, L., Yao, X.S., 2014. Metabolites profile of Xian-Ling-Gu-Bao capsule, a traditional Chinese medicine prescription, in rats by ultra performance liquid chromatography coupled with quadrupole time-of-flight tandem mass spectrometry analysis. J. Pharm. Biomed. Anal. 96, 90–103. https://doi.org/10.1016/j.jpba.2014.03.024.

Gfeller, D., Grosdidier, A., Wirth, M., Daina, A., Michielin, O., Zoete, V., 2014. SwissTargetPrediction: a web server for target prediction of bioactive small molecules. Nucleic Acids Res. 42 (W1), W32–W38. https://doi.org/10.1093/nar/gku293.

Guruswamy, R., ElAli, A., 2017. Complex roles of microglial cells in ischemic stroke pathobiology: new insights and future directions. Int. J. Mol. Sci. 18 (3), 496. https://doi.org/10.3390/ijms18030496.

Jiang, J., Song, J., Jia, X.B., 2015. Phytochemistry and ethnopharmacology of Epimedium L. species. Chin. Herb. Med. 7 (3), 204–222. https://doi.org/10.1016/S1674-6384(15)60043-0.

Jin, J., Wang, H., Hua, X.Y., Chen, D.J., Huang, C., Chen, Z., 2019. An outline for the pharmacological effect of icariin in the nervous system. Eur. J. Pharmacol. 842, 20–32. https://doi.org/10.1016/j.ejphar.2018.10.006.

Kalaria, R.N., Akinyemi, R., Ihara, M., 2016. Stroke injury, cognitive impairment and vascular dementia. Biochim. Biophys. Acta Mol. Basis Dis. 1862 (5), 915–925. https://doi.org/10.1016/j.bbadis.2016.01.01.

Kuriakose, D., Xiao, Z., 2020. Pathophysiology and treatment of stroke: present status and future perspectives. Int. J. Mol. Sci. 21 (20), 7609. https://doi.org/10.3390/ijms21207609.

Li, C., Li, Q., Mei, Q.B., Lu, T.L., 2015. Pharmacological effects and pharmacokinetic properties of icariin, the major bioactive component in Herba Epimedii. Life Sci. 126, 57–68. https://doi.org/10.1016/j.lfs.2015.01.006.

Li, C., Du, X., Liu, Y., Liu, Q.Q., Zhi, W.B., Wang, C.L., Zhou, J., Zhang, H., 2020a. A systems pharmacology approach for identifying the multiple mechanisms of action for the Rougui-Fuzi herb pair in the treatment of cardiocerebral vascular diseases. Evid. Based Complement. Alternat. Med. 2020 (1), 5196302. https://doi.org/10.1155/2020/5196302.

Li, C., Jia, W.W., Yang, J.L., Cheng, C., Olaleye, O.E., 2022. Multi-compound and drug-combination pharmacokinetic research on Chinese herbal medicines. Acta Pharmacol. Sin. 43 (12), 3080–3095. https://doi.org/10.1038/s41401-022-00983-7.

Li, L.X., Scott, C.A., Rothwell, P.M., 2020b. Trends in stroke incidence in high-income countries in the 21st century. Stroke. 51 (5), 1372–1380. https://doi.org/10.1161/STROKEAHA.119.028484.

Lin, Y., Yang, L., Yang, X., Qiu, C., Zhang, Y., 2013. Clinical curative effect in depression patients with kidney deficiency and liver stagnation treated with kidney-tonifying and depression resolving method. Chin. Arch. Tradit. Chin. Med. 31 (10), 2143–2145. https://10.13193/j.issn.1673-7717.2013.10.029.

Lu, M., Wang, L.H., Luo, Y.W., Ge, J.R., Gao, S.T., Chen, J.Y., Yang, F.Y., Shen, L., 2013. Treatment of primary osteoporosis with epimedium total flavone capsule: a multicenter clinical observation on 360 cases. Chin. J. Osteoporos. 19 (3), 279–282. https://doi.org/10.3969/j.issn.1006-7108.2013.03.019.

Ma, H.P., He, X.R., Yang, Y., Li, M.X., Hao, D.J., Jia, Z.P., 2011. The genus Epimedium: an ethnopharmacological and phytochemical review. J. Ethnopharmacol. 134 (3), 519–541. https://doi.org/10.1016/j.jep.2011.01.001.

Mijajlović, M.D., Pavlović, A., Brainin, M., Heiss, W.D., Quinn, T.J., Ihle-Hansen, H.B., Hermann, D.M., Assayag, E.B., Richard, E., Thiel, A., Kliper, E., Shin, Y.I., Kim, Y.H., Choi, S., Jung, S., Lee, Y.B., Sinanović, O., Levine, D.A., Schlesinger, I., Mead, G., Milošević, V., Leys, D., Hagberg, G., Ursin, M.H., Teuschl, Y., Prokopenko, S., Mozheyko, E., Bezdenezhnykh, A., Matz, K., Aleksić, V., Muresanu, D., Korczyn, A. D., Bornstein, N.M., 2017. Post-stroke dementia – a comprehensive review. BMC Med. 15 (1), 1–12. https://doi.org/10.1186/s12916-017-0779-7.

Qian, H.Q., Wu, D.C., Li, C.Y., Liu, X.R., Han, X.K., Peng, Y., Zhang, H., Zhao, B.Y., Zhao, Y., 2024. A systematic review of traditional uses, phytochemistry, pharmacology and toxicity of Epimedium koreanum Nakai. J. Ethnopharmacol. 318, 116957. https://doi.org/10.1016/j.jep.2023.116957.

Qin, J., Xiang, G.L., Gao, H.M., Meng, X.L., Wang, S.H., Zhang, Y., 2024. Determination of the pharmacodynamic substances and mechanism of Shiwuwei Saierdou Pills against cholestatic hepatitis through chemical profile identification and network pharmacology analysis. Arab. J. Chem. 17 (2), 105504. https://doi.org/10.1016/j.arabjc.2023.105504.

Shabab, T., Khanabdali, R., Moghadamtousi, S.Z., Kadir, H.A., Mohan, G., 2017. Neuroinflammation pathways: a general review. Int. J. Neurosci. 127 (7), 624–633. https://doi.org/10.1080/00207454.2016.1212854.

Shao, L., Zhang, B., 2013. Traditional Chinese medicine network pharmacology: theory, methodology and application. Chin. J. Nat. Med. 11 (2), 110–120. https://doi.org/10.1016/S1875-5364(13)60037-0.

Szabó, R., Rácz, C.P., Dulf, F.V., 2022. Bioavailability improvement strategies for icariin and its derivates: a Review. Int. J. Mol. Sci. 23 (14), 7519. https://doi.org/10.3390/ijms23147519.

Van Der Flier, W.M., Skoog, I., Schneider, J.A., Pantoni, L., Mok, V., Chen, C.L., Scheltens, P., 2018. Vascular cognitive impairment. Nat. Rev. Dis. Primers 4 (1), 1–16. https://doi.org/10.1038/nrdp.2018.3.

Van Hasselt, J.C., Iyengar, R., 2019. Systems pharmacology: defining the interactions of drug combinations. Annu. Rev. Pharmacol. Toxicol. 59, 21–40. https://doi.org/10.1146/annurev-pharmtox-010818-021511.

Vezzani, A., Balosso, S., Ravizza, T., 2019. Neuroinflammatory pathways as treatment targets and biomarkers in epilepsy. Nat. Rev. Neurosci. 15 (8), 459–472. https://doi.org/10.1038/s41582-019-0217-x.

Wang, X.J., 2002. Studies on serum pharmacochemistry of traditional Chinese medicine. World Sci. Technol. 4 (2), 1–5.

Woodburn, S.C., Bollinger, J.L., Wohleb, E.S., 2021. The semantics of microglia activation: neuroinflammation, homeostasis, and stress. J. Neuroinflammation 18 (1), 1–16. https://doi.org/10.1186/s12974-021-02309-6.

Wu, X.Y., Wei, J.J., Yi, Y., Shu, G.T., He, Z.X., Gong, Q.H., Gao, J.M., 2023. Epimedium aqueous extract ameliorates cerebral ischemia/reperfusion injury through inhibiting ROS/NLRP3-mediated pyroptosis. Antioxidants 12 (5), 999. https://doi.org/10.3390/antiox12050999.

Wu, S., Wu, B., Liu, M., Chen, Z., Wang, W., Anderson, C.S., Sandercock, P., Wang, Y., Huang, Y., Cui, L., Pu, C., Jia, J., Zhang, T., Liu, X., Zhang, S., Xie, P., Fan, D., Ji, X., Wong, K.S.L., Wang, L., Wei, C., Wang, Y., Cheng, Y., Liu, Y., Li, X., Dong, Q., Zeng, J., Peng, B., Xu, Y., Yang, Y., Wang, Y., Zhao, G., Wang, W., Xu, Y., Yang, Q., He, Z., Wang, S., You, C., Gao, Y., Zhou, D., He, L., Li, Z., Yang, J., Lei, C., Zhao, Y., Liu, J., Zhang, S., Tao, W., Hao, Z., Wang, D., Zhang, S., 2019. Stroke in China: advances and challenges in epidemiology, prevention, and management. Lancet Neurol. 18 (4), 394–405. https://doi.org/10.1016/S1474-4422(18)30500-3.

Xiang, G.L., Yang, L.Y., Qin, J., Wang, S.H., Zhang, Y., Yang, S.J., 2024. Revealing the potential bioactive components and mechanism of Qianhua Gout Capsules in the treatment of gouty arthritis through network pharmacology, molecular docking and pharmacodynamic study strategies. Heliyon 10 (10), e30983.

Xie, C.C., Tang, H., Liu, G., Li, C.Q., 2022. Molecular mechanism of Epimedium in the treatment of vascular dementia based on network pharmacology and molecular docking. Front. Aging Neurosci. 14, 940166. https://doi.org/10.3389/fnagi.2022.940166.

Xu, Z.K., Yin, H.M., Li, F., Qin, J.P., Gu, S.L., Wu, Y., Wang, Z.Z., Xiao, W., 2018. Determination of flavonoids constituents in epimedium total flavone capsule and research on its anti-osteoporosis activity. Chin. J. Chin. Mater. Med. 43 (15), 3140–3144. https://doi.org/10.19540/j.cnki.cjcmm.20180611.003.

Xu, H., You, M., Xiang, X., Zhao, J., Yuan, P., Chu, L., Xie, C., 2022. Molecular mechanism of Epimedium extract against ischemic stroke based on network pharmacology and experimental validation. Oxid. Med. Cell Longev. 2022, 3858314. https://doi.org/10.1155/2022/3858314.

Yang, P.X., Fan, X.X., Liu, M.U., Liu, J., Cao, L., Wang, Z.Z., Wang, X., Zhang, X.Z., Xiao, W., 2024. Effects of epimedium total flavone capsules on post-stroke cognitive impairment in rats. Chin. J. Chin. Mater. Med. 49 (8), 2262–2272. https://doi.org/10.19540/j.cnki.cjcmm.20240118.104.

Zhang, D.W., Liu, L., Jia, Z.B., Yao, X.S., Yang, M.S., 2016. Flavonoids of herba Epimedii stimulate osteogenic differentiation and suppress adipogenic differentiation of primary mesenchymal stem cells via estrogen receptor pathway. Pharm. Biol. 54 (6), 954–963. https://doi.org/10.3109/13880209.2015.1079224.

Zhang, X.L., Tang, B.L., Wen, S.J., Wang, Y.T., Pan, C.X., Qu, L.B., Yin, Y.L., Wei, Y.J., 2023. Advancements in the biotransformation and biosynthesis of the primary active flavonoids derived from Epimedium. Molecules 28 (20), 7173. https://doi.org/10.3390/molecules28207173.

Zhao, L., Zhang, H., Li, N., Chen, J.M., Xu, H., Wang, Y.J., Liang, Q.Q., 2023. Network pharmacology, a promising approach to reveal the pharmacology mechanism of Chinese medicine formula. J. Ethnopharmacol 309, 116306. https://doi.org/10.1016/j.jep.2023.116306.

Zhou, J., Chen, Y., Wang, Y., Gao, X., Qu, D., Liu, C., 2013. A comparative study on the metabolism of Epimedium koreanum Nakai-prenylated flavonoids in rats by an intestinal enzyme (Lactase Phlorizin Hydrolase) and intestinal flora. Molecules 19 (1), 177–203. https://doi.org/10.3390/molecules19010177.